E949 Technical Note K-065

The Active Degrader

Ilektra A. Christidi, Stony Brook

November 20, 2006

Abstract

The Active Degrader (AD) has not been used in the PNN1 analysis, but is essential for PNN2, given the expected photon distribution from target-scattered Kp2 events, which is uniform in dip angle ([1], fig. 2 and 3). In this note, the energy calibration and time slewing corrections applied to the AD will be reviewed, the photon signature in this subsystem and the optimization of the PV cut will be described and its correlation with other PV systems will be investigated. A net rejection gain of about 2 can be achieved when the AD is used, after all other PV has been applied.

1 Energy calibration

In the following, "energies" are in arbitrary units. For the CCDs they are the pulse height (average of the 2 highest bins of the pulse found by the pulse.f routine) and they have been calibrated with respect to each other and pedestal-corrected for multiple hits in one CCD. The pedestal correction was determined by fitting to a Gaussian the sum of the "energies" of every hit, for events with different total number of hits. The sample used was Km2's with good activity at BM time and no activity at TRS in the beam systems. It was observed that for every extra hit, the energy peak mean moved by a certain amount, as shown in figures 1-3 and listed in table 1. As no requirement was imposed for the number of sectors hit by the passing Kaon, most of the events with multiple hits include more than one sectors, hit at similar (BM) times. Therefore a time-dependent CCD baseline is unlikely to be the cause of the energy shift. The correction was verified to work with Kp2 peak events, for which the energy peak for incoming Kaons was stable as a function of element number and number of hits after the pedestal correction was applied (see fig. 4).

hit #	pedestal
1	0.
2	20.446
3	14.267
4	14.393
5	12.244
6	10.383
7	7.574
8	10.848
9	8.431
10	10.801
11	4.733
12	7.196
13	15.588
14	11.121
15 or more	5.641

Table 1: CCD pedestal correction (in arbitrary CCD units) for every extra hit. Note that the pedestal value in general decreases the more hits are added (see explanation in the text). For 15 hits or more, the average value is used.

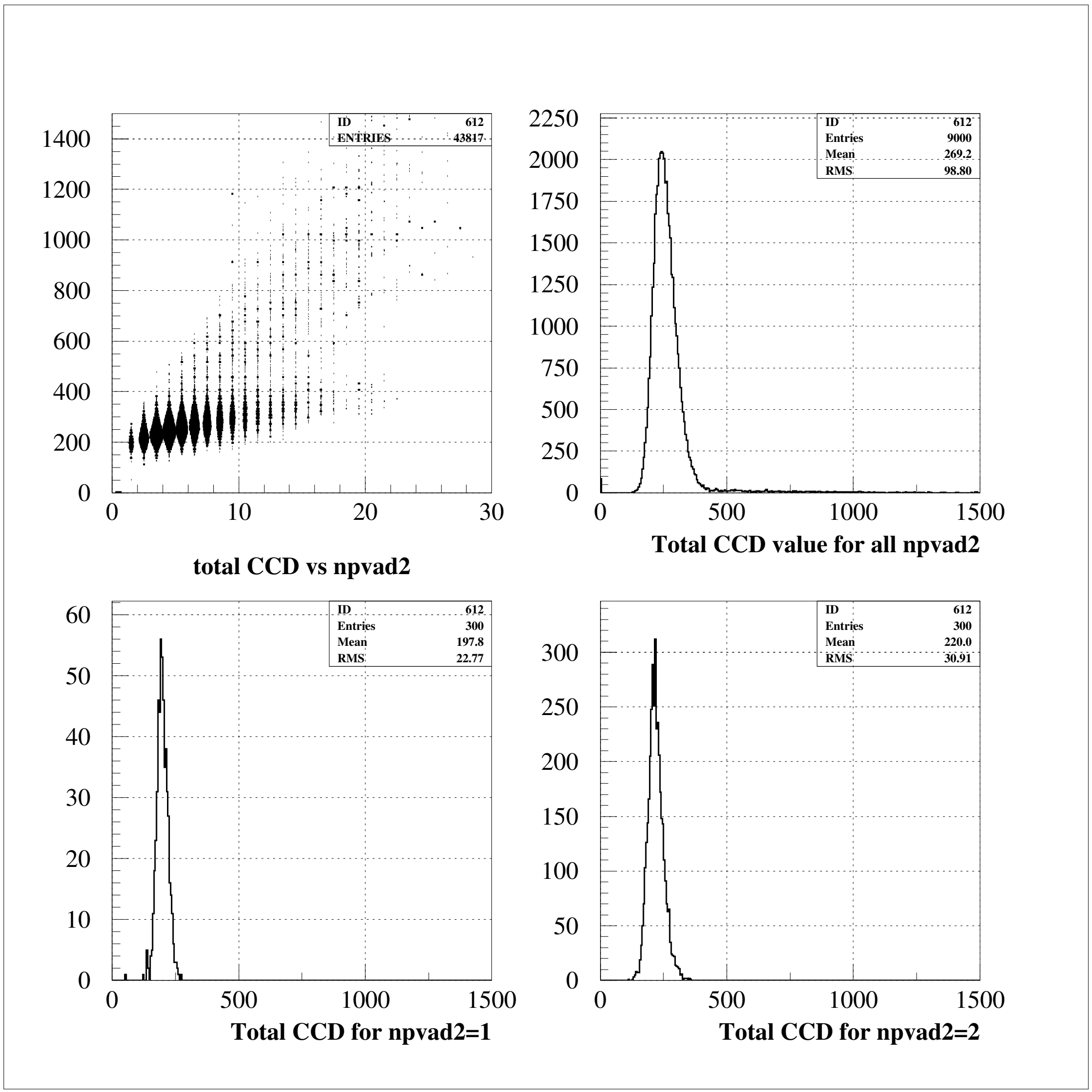

Figure 1: Total CCD "energy" vs number of CCD hits (upper left) and CCD "energy" projection (upper right) for all numbers of hits. The rest of the plots are for different (1-2) number of CCD hits (continues in the next 2 figures). An increase of the mean of the energy peak is evident for every extra hit. The events used are Km2's with no activity in the beam elements at TRS.

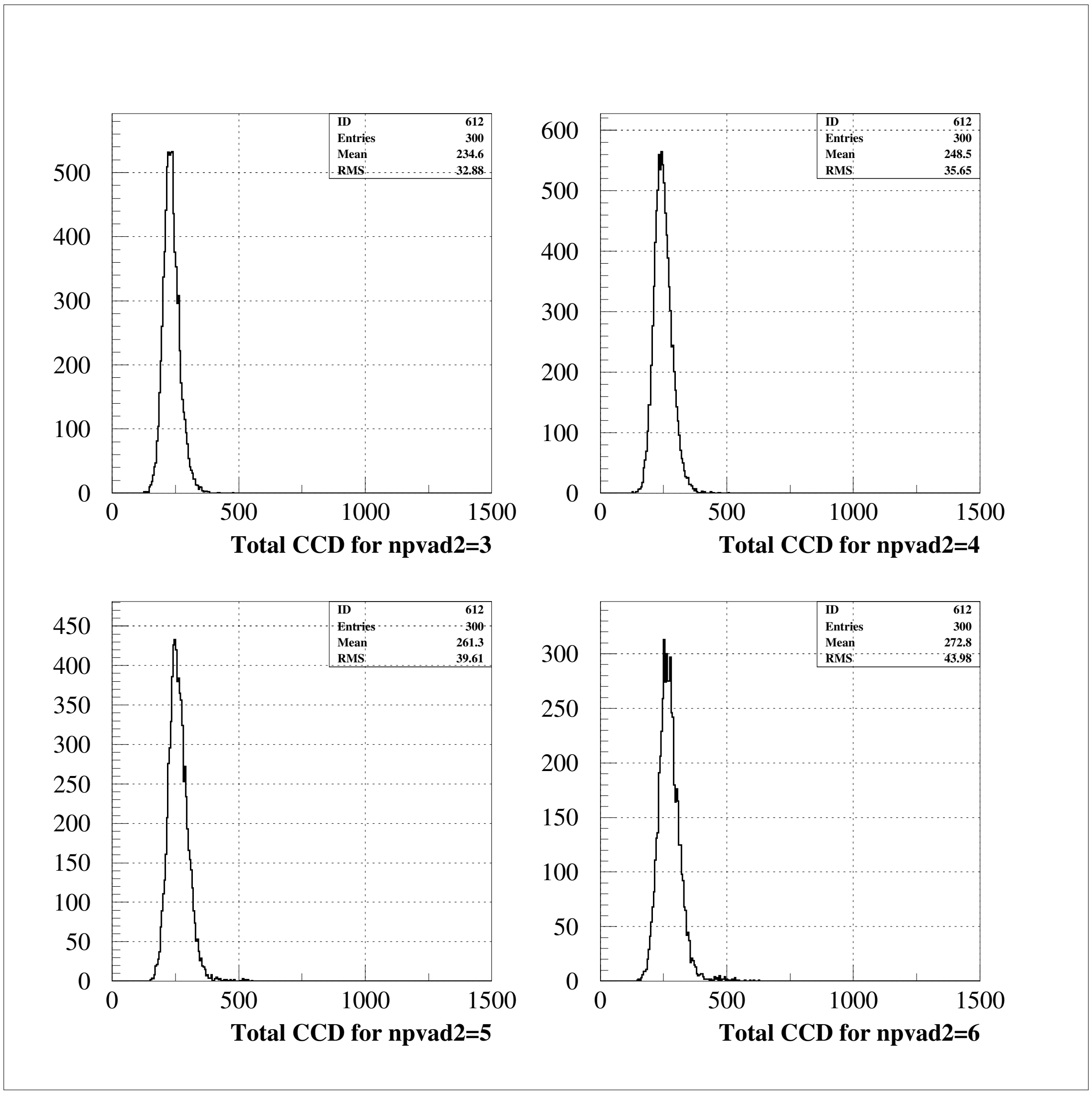

Figure 2: Total CCD "energy" for different (3-6) number of CCD hits, where an increase of the mean of the energy peak is evident for every extra hit. The events used are Km2's with no activity in the beam elements at TRS.

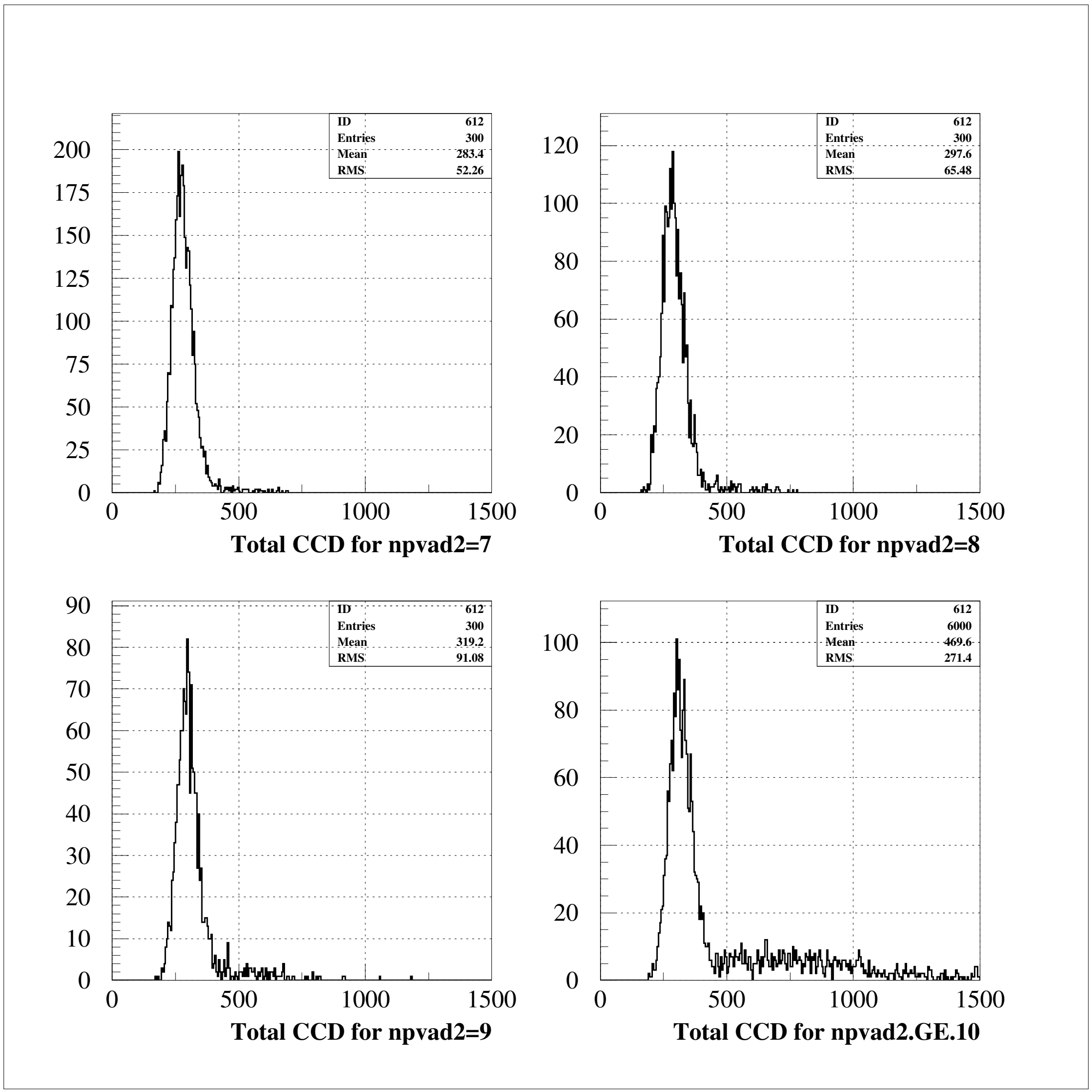

Figure 3: Total CCD "energy" for different (7-10) number of CCD hits, where an increase of the mean of the energy peak is evident for every extra hit. The events used are Km2's with no activity in the beam elements at TRS.

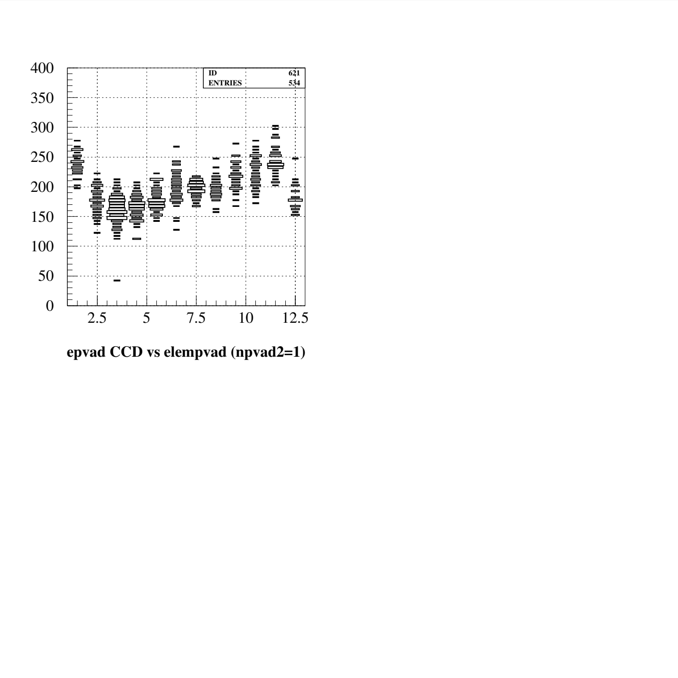

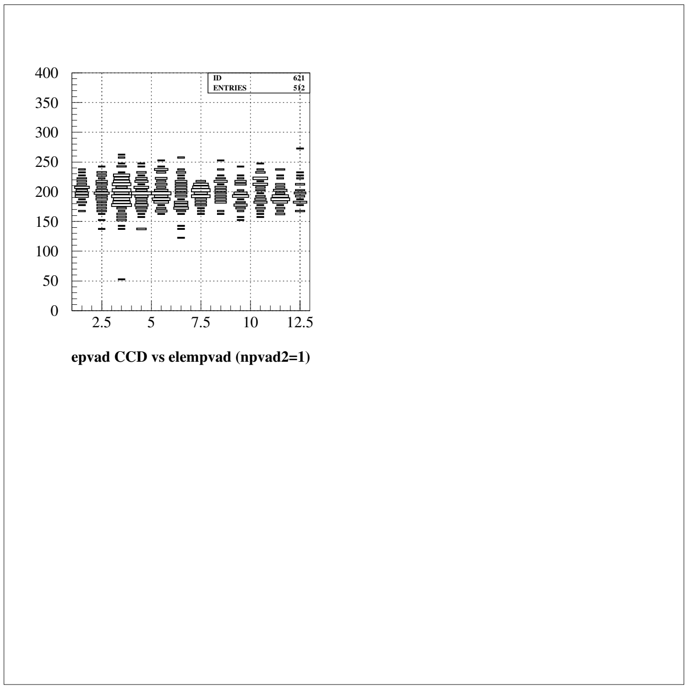

Figure 4: Incoming Kaon CCD energy peak position for every element number before (top) and after (bottom) the pedestal correction and relative element calibration.

For the ADCs, the "energy" values are the ADC hit values, also calibrated with respect to each other and then de-multiplexed based on the CCD information: the CCD energy of all hits in every sector, as well as in every ADC multiplexed unit, is summed, after they have been corrected as described in the previous paragraph. Then their ratio gives the contribution of every sector to the ADC energy. This way an ADC value is assigned to every sector (not every hit, unlike the CCD), and finally it is corrected also for the energy lost in dead material when multiple sectors are crossed. This effect was observed as a down-shift of about 13 (in ADC units) in the Kaon energy peak for every extra sector crossed, for Km2's (see figures 5-6). Note that there is usually only one TDC hit for every sector (whereas there are multiple CCD ones), therefore the number of hits in an event is equivalent to the number of sectors hit.

For the CCDs, the energy loss correction is absorbed in the pedestal subtraction, as the two factors contribute simultaneously to the increase/decrease of the energy as a function of number of hits. This is probably the reason why the CCD pedestal correction varies with the number of hits.

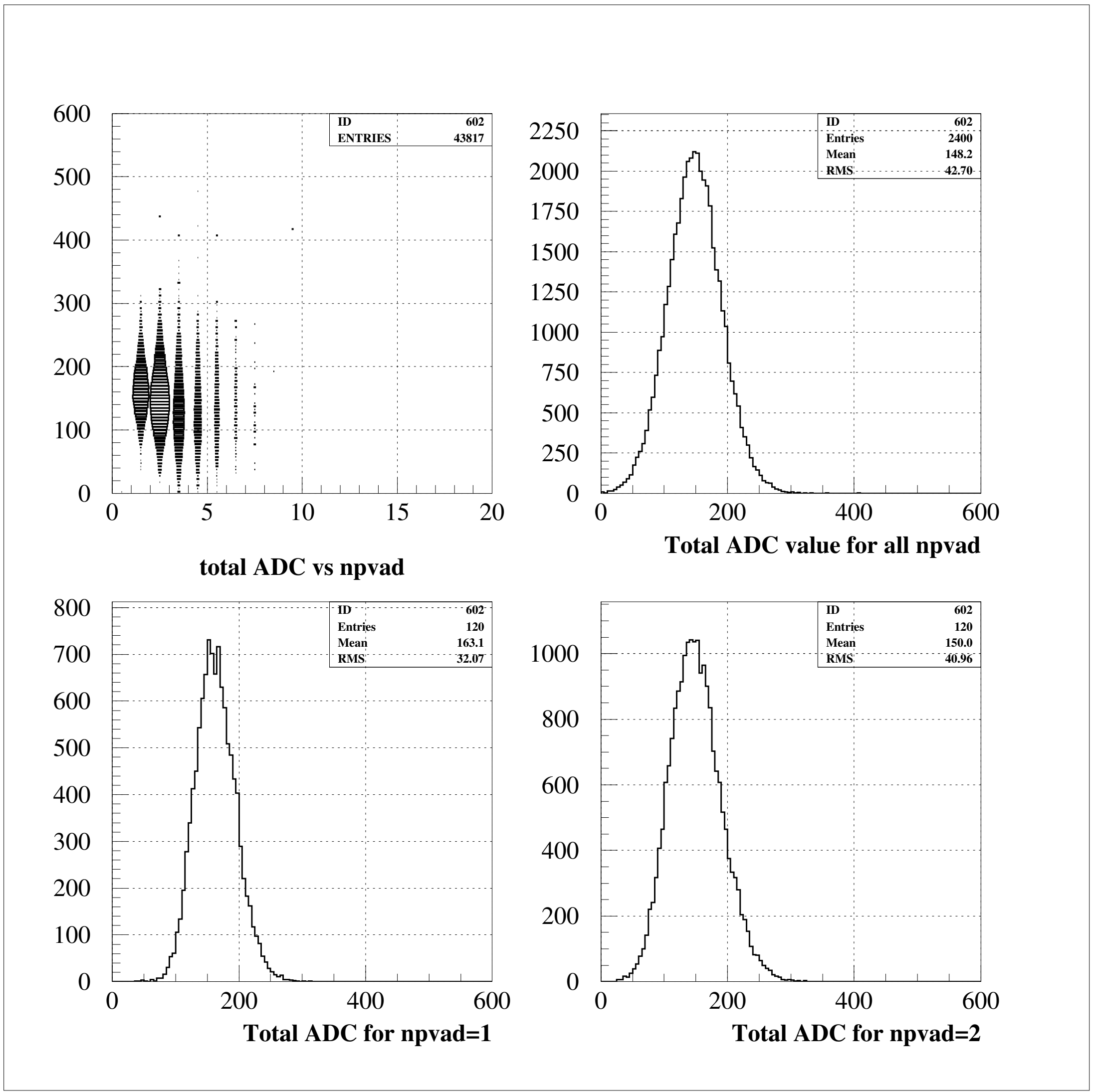

Figure 5: Total ADC "energy" vs number of TDC hits (upper left) and ADC "energy" projection (upper right) for all numbers of hits. The rest of the plots are for different (1-2) number of TDC hits (continues in the next figure). A decrease of the mean of the energy peak is evident for every extra hit (or sector). The events used are Km2's with no activity in the beam elements at TRS.

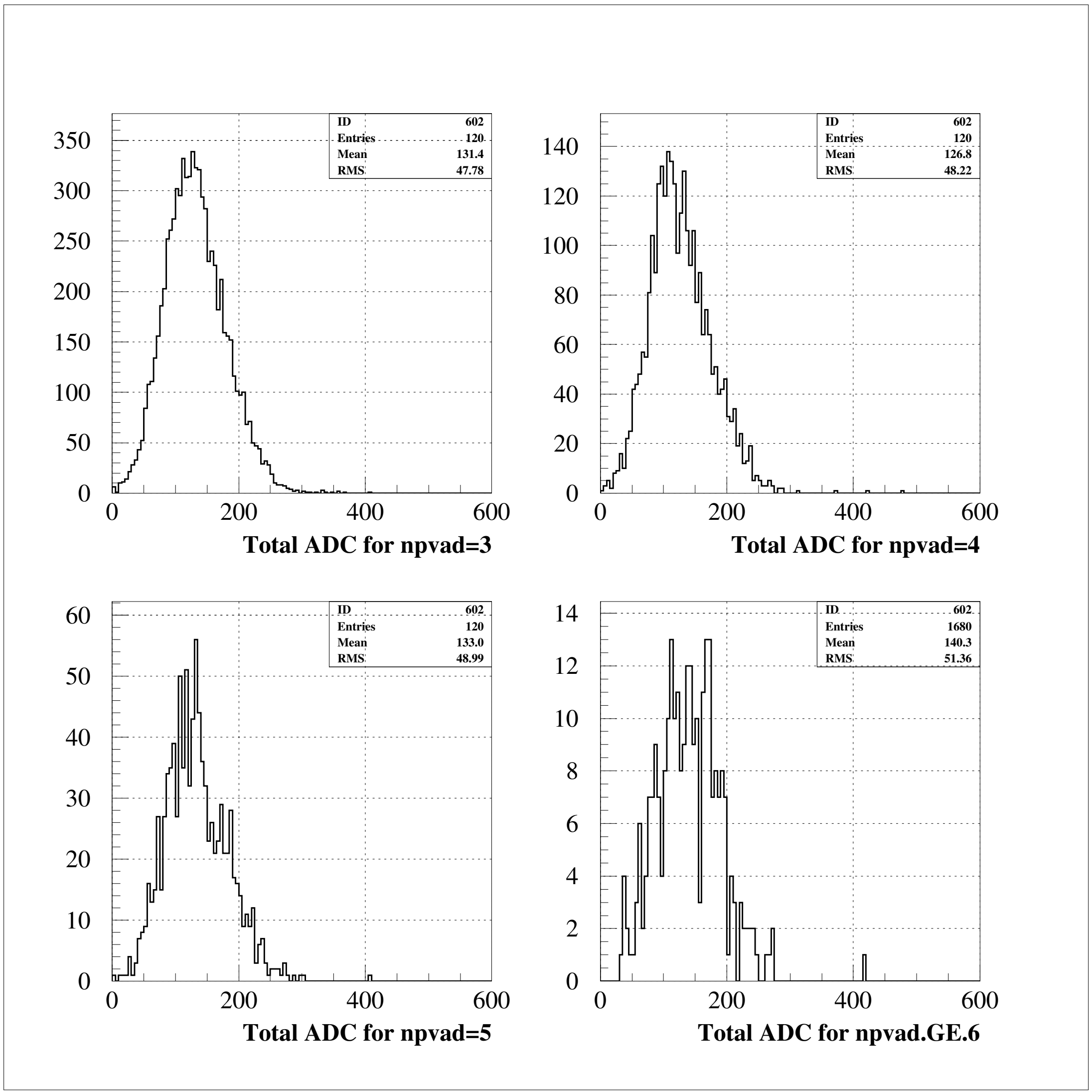

Figure 6: Total ADC "energy" for different (3-6) number of TDC hits. A decrease of the mean of the energy peak is evident for every extra hit (or sector). The events used are Km2's with no activity in the beam elements at TRS.

In order to find the energy in MeV, the method from [2] was used for pions, as a validation. The fits for data (this study) and simulation ([3]) are shown in fig. 7 and the results in table 2. Comparing with the results for Kaons in [2], we can see that they are consistent, therefore a calibration constant of 6.34 ADC hits/MeV (the average for Kaon and pion narrow fit) can be used to translate the energy plots in this note to MeV.

2 Time slewing corrections and time calibration

When slewing corrections based on the incoming beam Kaon were applied to the TDCs, the time resolution neither for the K nor for the photon was improved significantly (see fig. 8 and 9). This might be due to several reasons:

Quantity	MC	Narrow	Wide
Mean	15.26±0.24 MeV	99.0±0.6 (ADC)	98.4±0.5 (ADC)
σ	2.154±0.198 MeV	41.9±0.6 (ADC)	46.8±0.5 (ADC)
σ(calib)	-	6.46 MeV	7.26 MeV
ADC/MeV	-	6.49	6.45
N_{pe}	-	6.28	4.85
N_{pe}/MeV	-	0.41	0.32

Table 2: The fit results, calibration and calculated average number of photoelectrons for pions. For more details, see [2].

(a) the K deposits most of its energy towards the DS of the AD, when it slows down, whereas the photons deposit it more towards the US, when they shower (or at least more uniformly in z than the K). Since we do not know the z-dependence of the gain, this can cause a slewing correction derived from K's (i.e. mostly from the DS) not to work for photons. To check this hypothesis, slewing corrections based on beam pions (that deposit energy more uniformly in z, and also deposit less energy in total, making them more similar to photons than Kaons are) were calculated. The results are shown in fig. 10 for the pion peak and fig. 11 for the photons. The improvement for both the pions and the photons is still marginal, but the correction will be applied because it improves the general quality of the timing peak (reduces the tails).

(b) the K beam is more or less centered at the AD, whereas the photons can be anywhere in xy. Since the gain changes by up to a factor of 3 from the center to the edge (see section 6), this can be another source of discrepancy, which could not be disentangled (we have no position information for the outgoing photons).

(c) the slewing corrections were derived from events in which the K transverses only one sector. This is not a representative sample, and an unknown amount of the energy could be lost in dead material (among other unpredictable features).

	K peak	π peak	γ peak
mean (ns)			
before corrections	-1.17±0.01	-0.2±0.02	3.09±0.10
after K-based corrections	-0.03±0.01	-	2.66±0.09
after π-based corrections	-0.64±0.01	-0.1±0.01	2.02±0.09
sigma (ns)			
before corrections	0.83±0.01	0.98±0.01	1.57±0.08
after K-based corrections	0.81±0.01	-	1.51±0.07
after π-based corrections	0.86±0.01	0.93±0.01	1.51±0.09

Table 3: Fitted mean and sigma of various timing peaks before and after slewing corrections. The numbers are taken from the fits in fig. 8-11.

The results of the Kaon- and pion-based slewing corrections for all timing peaks are summarized in table 3. From these numbers it is obvious that the AD timing was calibrated with beam pions, which have $\beta_{US} = 0.98$ at the US face of the AD and $\beta_{DS} = 0.96$ at the DS one. This is why the

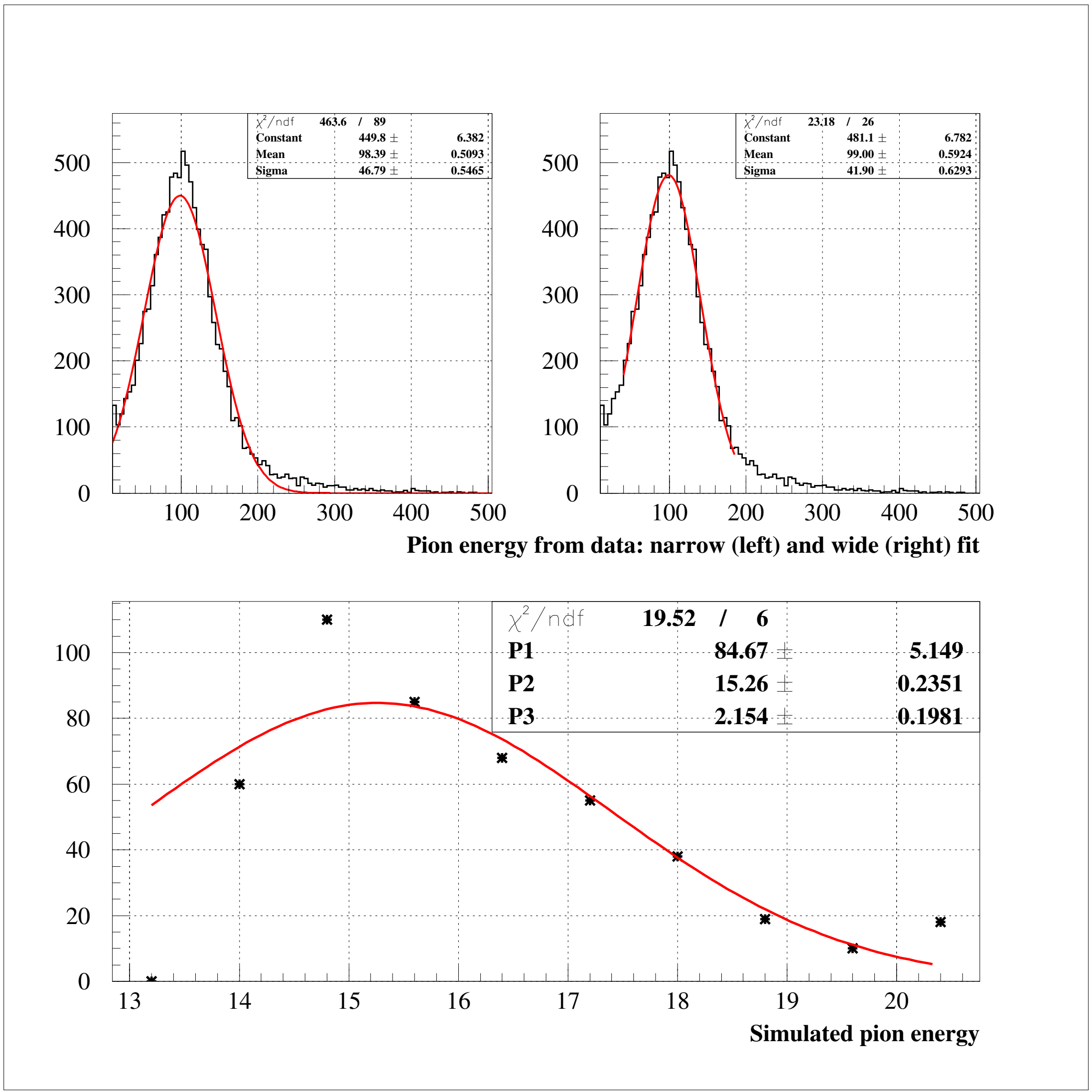

Figure 7: The fits to pion energy distributions for data (wide and narrow range) and MC ([3]).

Kaons, with $\beta_{US} = 0.77$ and $\beta_{DS} = 0.48$, come 0.6ns earlier than the pions with respect to tk in the target after slewing corrections: this is the extra time the Kaons take to slow down in the AD and stop in the target.

Given that the beam pions take about 1.2ns to cross the AD ($\sim$18 cm long) and reach the center of the target (another $\sim$16 cm) at this speed, and assuming that tk is given mostly by the fibers near the stopping fiber (it is an energy-weighted average, and most of the Kaon energy is deposited at the end of its track), then the AD timing is calibrated by this amount. Therefore, the photons traveling back to the AD should be expected to reach its US face about 1ns after tpi (the TOF, see fig. 12) plus this 1.2ns correction, which is very close to the 2.02ns offset found after the pion-based slewing corrections. (Take into account that the pion stopping time is not totally calibrated out, there is -0.1ns remaining, and that photons do not have to shower at the very US of the AD, although close to it, and the small discrepancy makes sense).

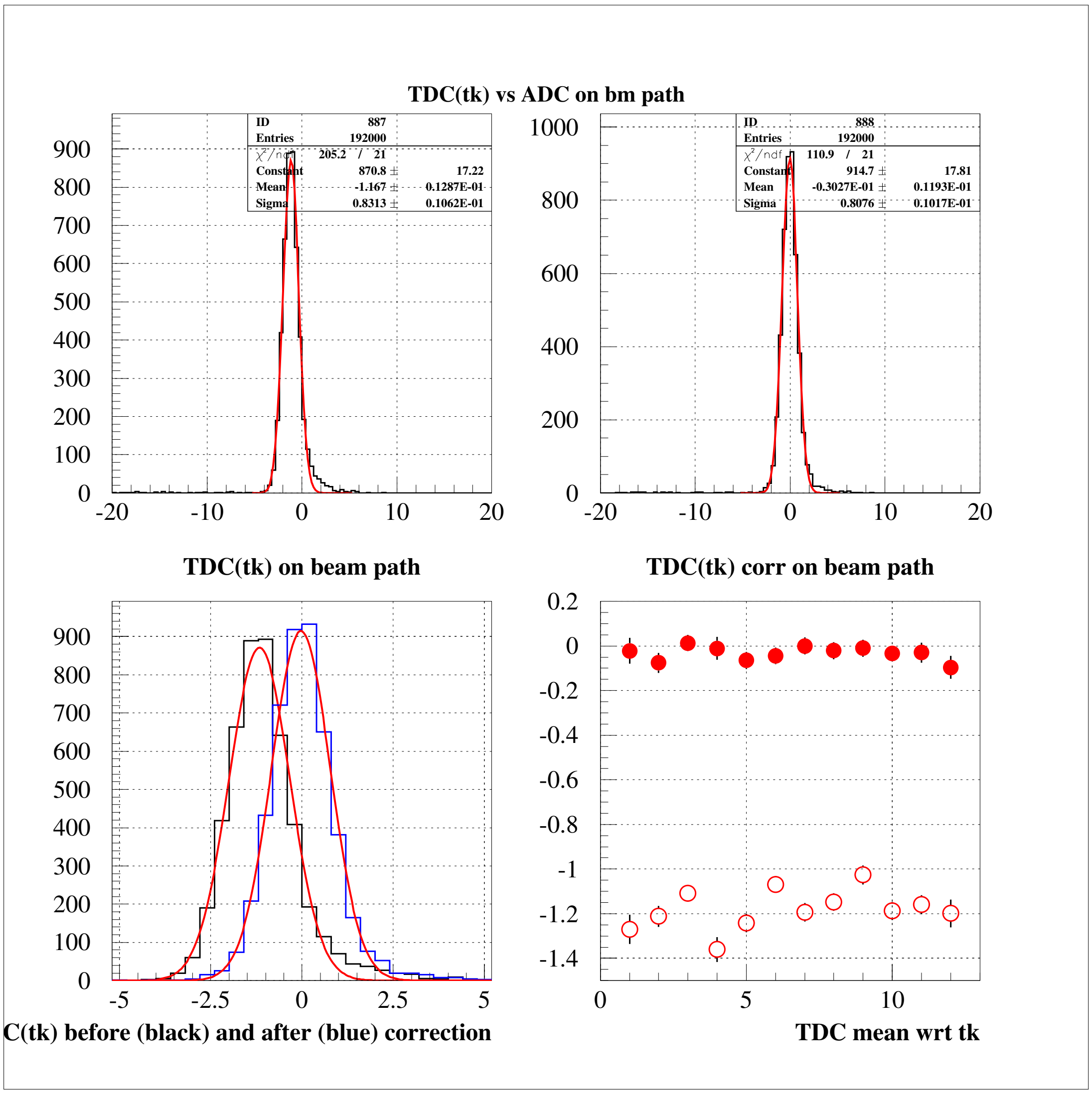

Figure 8: TDC timing peak at tk for incoming Kaons before (upper left) and after (upper right) Kaon-based slewing corrections for Km21s. The two distributions are overlayed in the lower left. The improvement in the resolution is about 20ps, with an error of 10ps. In the lower right plot, the fitted mean of the TDC distribution at tk for Kaons is shown for every sector, before (open circles) and after (closed circles) slewing corrections. The errors are the errors on the mean.

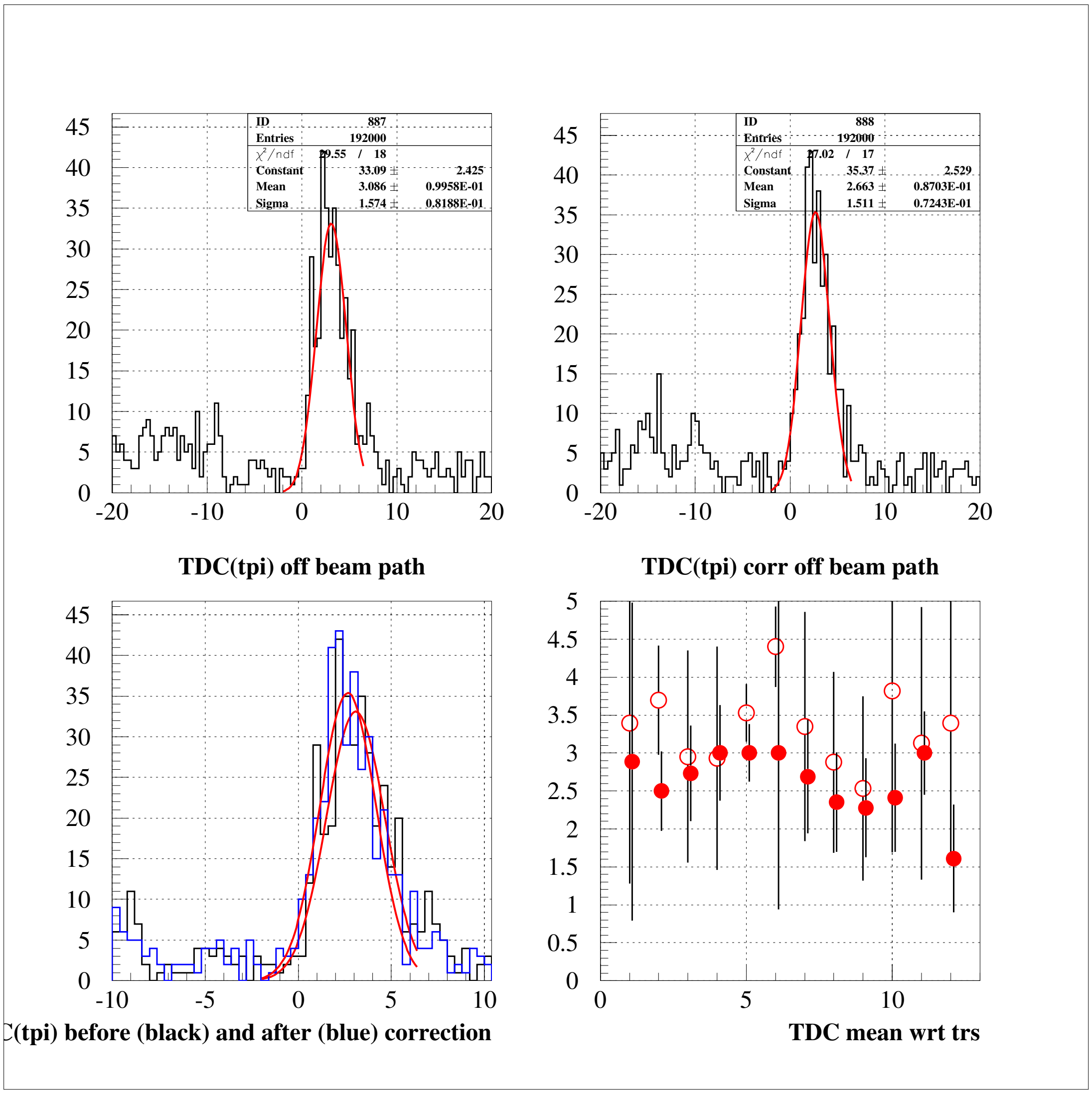

Figure 9: TDC timing peak at tpi for sectors not hit by the incoming Kaons before (upper left) and after (upper right) Kaon-based slewing corrections for Kp2 peak. The two distributions are overlayed in the lower left. The improvement in the resolution is about 60ps, with an error of 70-80ps. In the lower right plot, the fitted mean of the TDC distribution at tpi for photons is shown for every sector, before (open circles) and after (closed circles) slewing corrections. The errors are the errors on the mean.

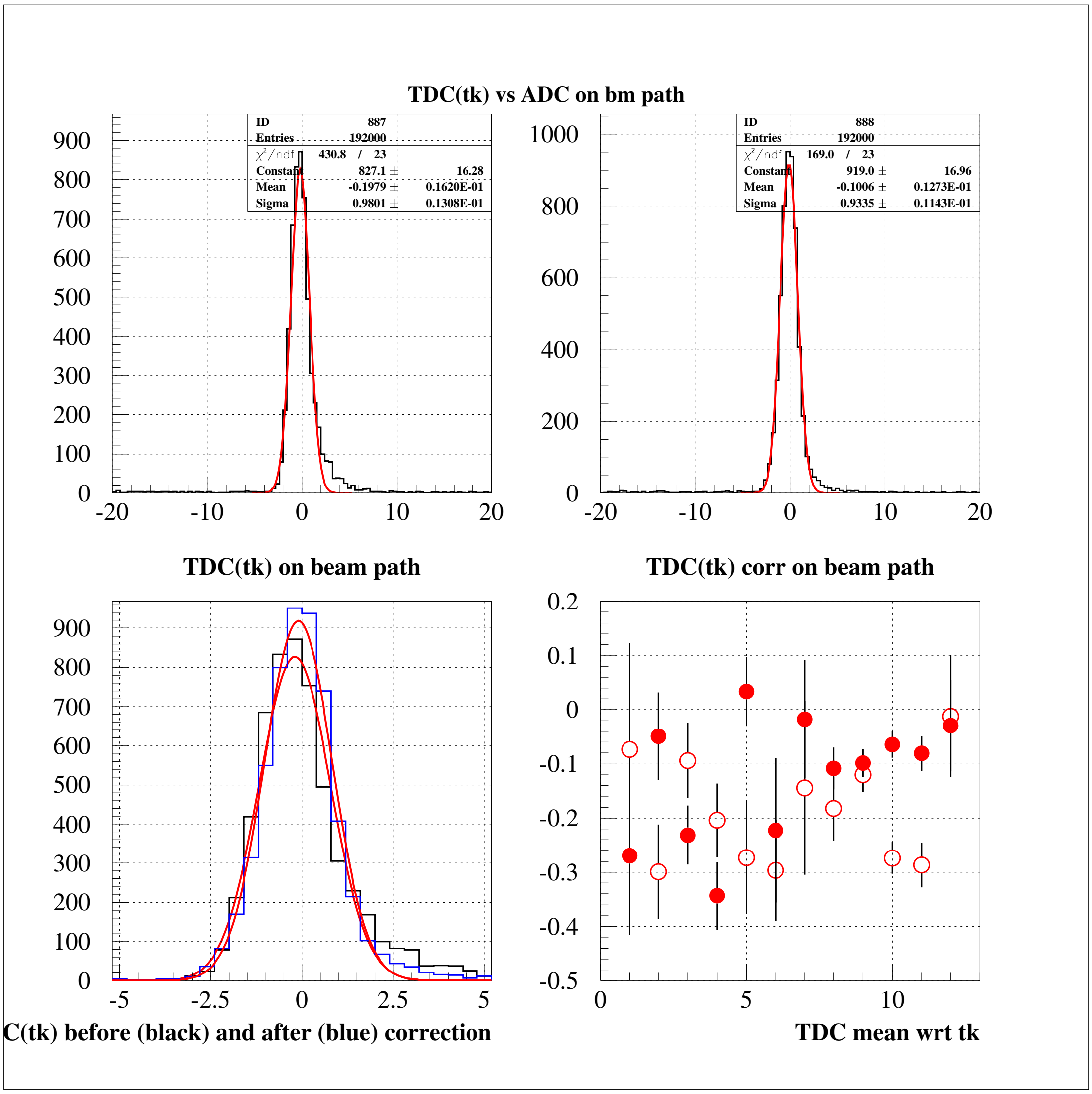

Figure 10: TDC timing peak at tk for incoming beam pions before (upper left) and after (upper right) pion-based slewing corrections for pbeam. The two distributions are overlayed in the lower left. The improvement in the resolution is about 50ps, with an error of 10ps. In the lower right plot, the fitted mean of the TDC distribution at tk for pions is shown for every sector, before (open circles) and after (closed circles) slewing corrections. The errors are the errors on the mean.

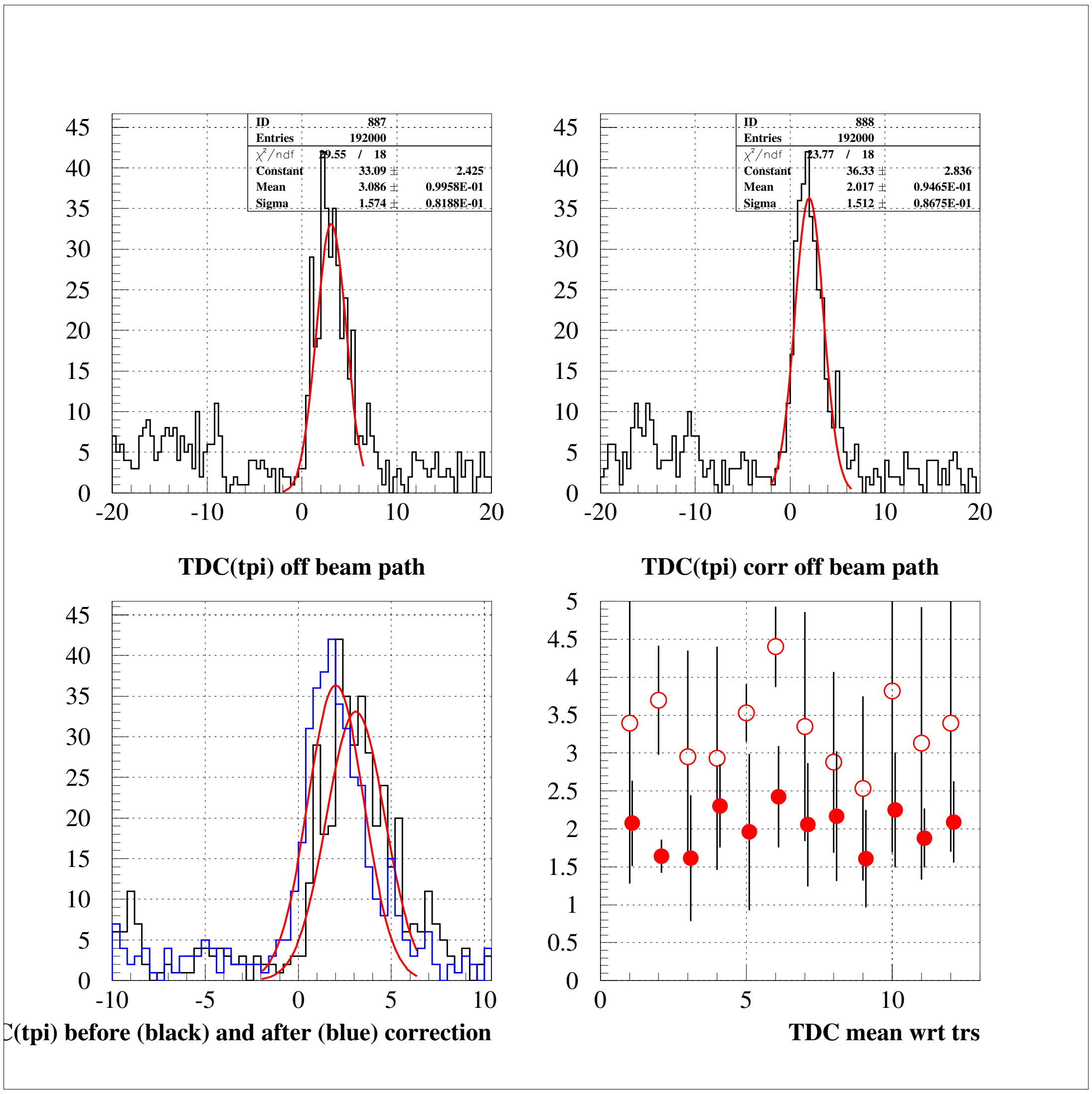

Figure 11: TDC timing peak at tpi for sectors not hit by the incoming Kaons before (upper left) and after (upper right) pion-based slewing corrections for Kp2 peak. The two distributions are overlayed in the lower left. The resolution improved by about 60ps, with an error of 80-90ps. In the lower right plot, the fitted mean of the TDC distribution at tpi for photons is shown for every sector, before (open circles) and after (closed circles) slewing corrections. The errors are the errors on the mean.

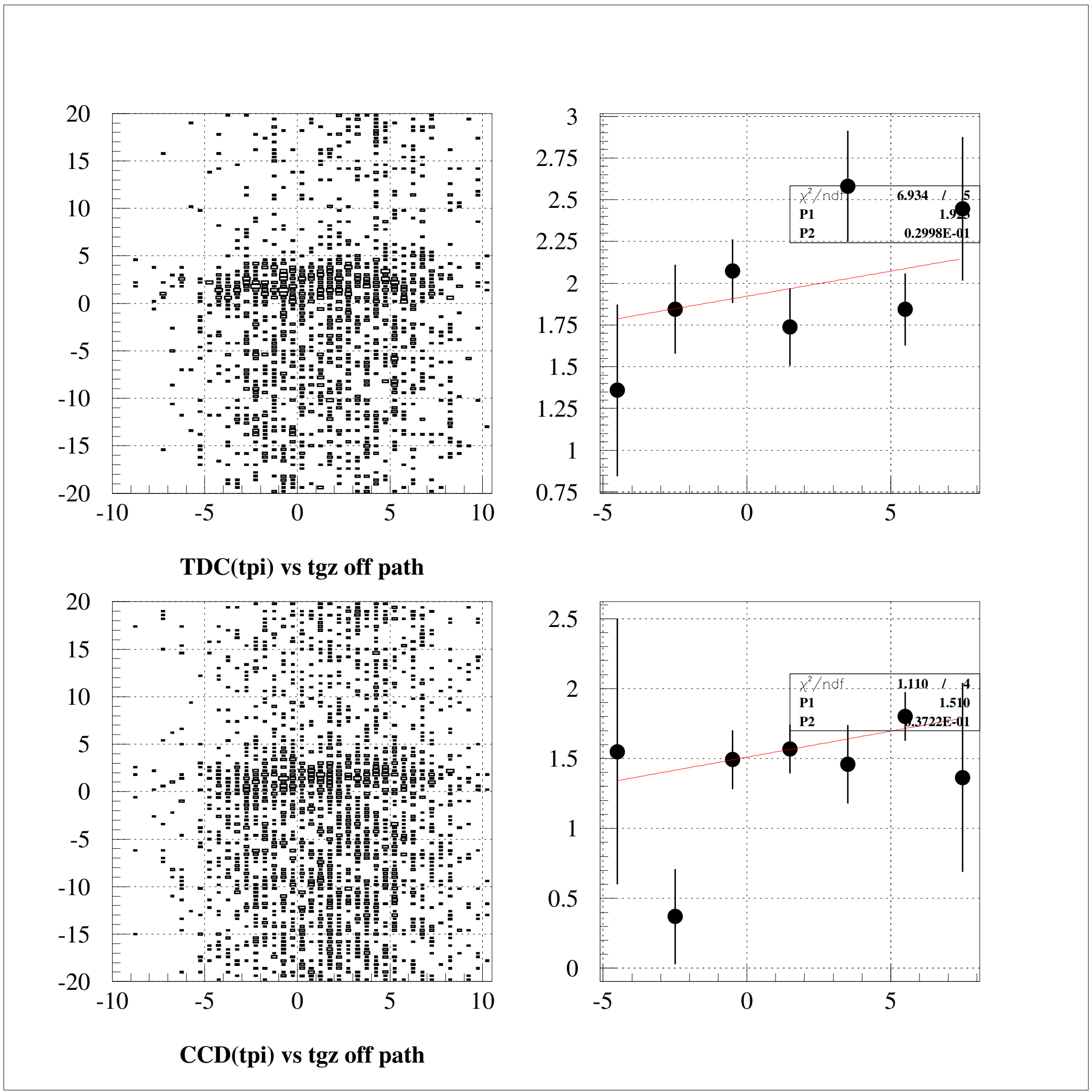

Figure 12: Dependence of the photon time peak position with respect to tpi, on tgz (and thus the distance the photons have to travel from the target until they reach the AD), for Kp2 peak events (B4EKZ has already been applied, therefore tgz is reliable). DELCO3 and an energy threshold of 5. has been applied. Scatter plots (left) and the result of fitting the peak in the limits -2ns to 6ns vs tgz (right) are shown for the TDCs in the top and CCDs in the bottom row. The error bars are the errors in the fitted mean. For both the TDCs and CCDs, it has a clear linear form, and the slope of the linear fit gives a reasonable speed of light value of about $3.3 \times 10^8 m/s$ and $2.7 \times 10^8 m/s$ respectively. (The second point of the CCD plot was not included in the fit in order to get a value close to the speed of light)

The relative timing between different sectors fluctuated from the average by about 200ps for beam Kaons before the slewing corrections, but it was taken care of by them, as they were done per-sector.

3 Other formalities

Beam particle track extrapolation is done to find which AD sectors are expected to be transversed by the incoming K, and thus have some energy deposit associated with the beam. In principle, these sectors should be excluded for PV purposes (more on that later). The incoming xy point is found by extrapolating the line defined by the hit points in BWC1 and BWC2 to the US face of the AD. The outgoing point is the one given by the B4 hit coordinates. Every sector between these 2 points is assigned to the K path. This algorithm has the flaw that it does not take into account the transverse uncertainty to the entering K point caused by multiple scattering in the Inactive Degrader (which is right US of the AD), which is exacerbated by the geometry of the AD: since the beam is centered where all the sectors meet, a small perturbation in the path causes more/other sectors than expected to be hit. A quantitative assessment of the efficiency of the method is given later.

The samples used in these studies are:

- Acceptance sample: Km21 monitors, with SKIM5 (without TDCUT), HEX afterburner, STLAY, KINCUTS, PSCUT02, TGCUTS, DELCO3, loose PVCUT and KMU2BOX, where no photon or beam activity is expected. **Events remaining: about 25,000**
- Rejection sample 1: Kp2 peak events from SKIM5 (without TDCUT), STLAY, KINCUTS, PSCUT02, TGCUTS, DELCO3, loose PVCUT and KPI2BOX. **Events remaining: 1693**
- Rejection sample 2: "good" (kink point in the target) kinks from SKIM8 with SKIM5 cuts (without TDCUT), STLAY, KINCUTS, PSCUT02_KINK, ring and US veto (RVUPV), $ptot < 225MeV/c$, loose TGCUTS, DELCO3 and loose PVCUT. **Events remaining: 608**

The kinematic quantities (rtot, ptot, etot and DELCO) of these samples are shown in fig. 13, before the PV and, for the first 3 quantities, before the BOX cut.

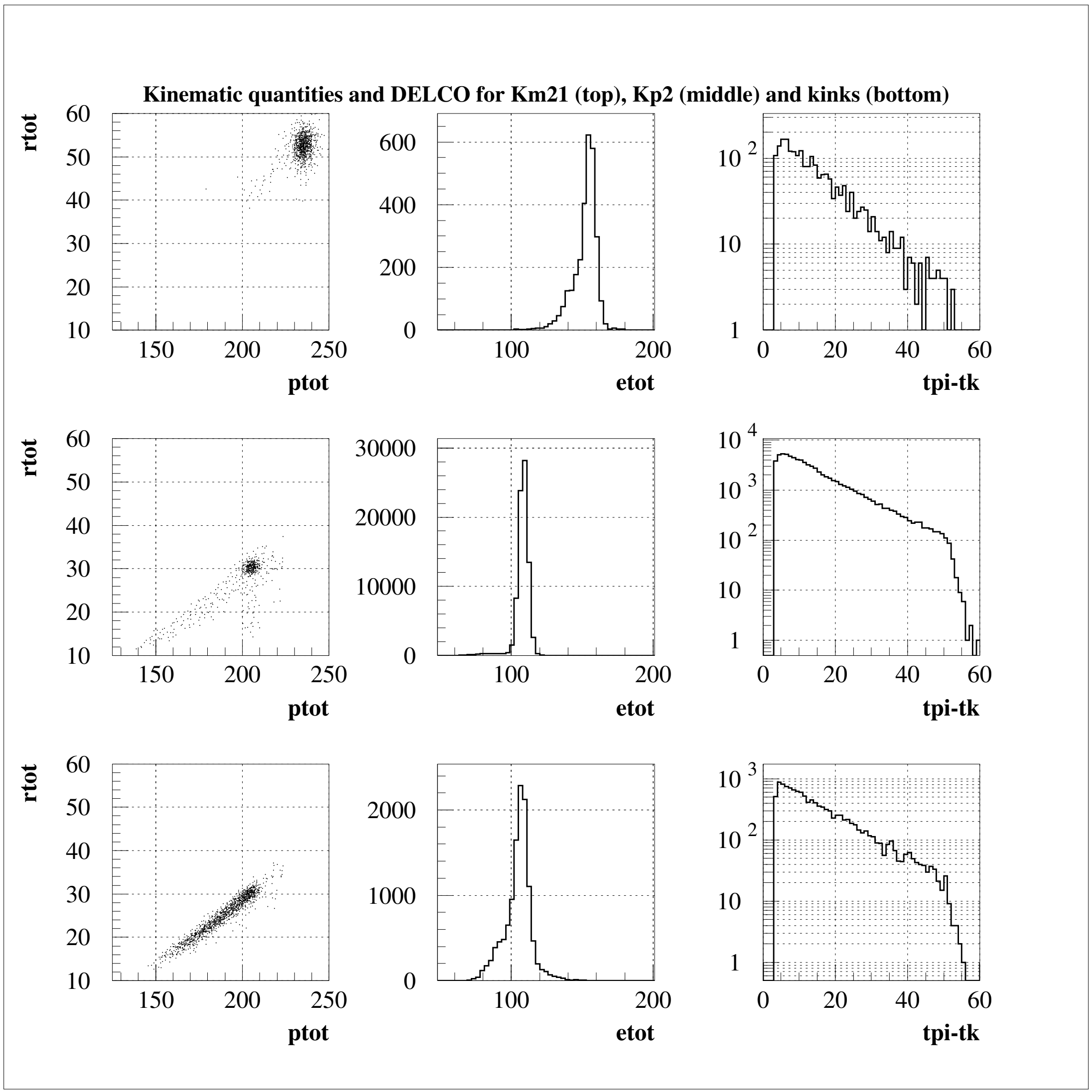

Figure 13: Kinematic distributions for the 3 samples used in this study: rtot vs ptot (left), etot (middle) and DELCO (right). The PV cut has not been applied for these plots, and for the 2 first columns the BOX cut has (obviously) not been applied either.

4 Timing peaks in the AD

In fig.14-17, the time distributions of hits in the AD are shown in black for the acceptance sample and red for the rejection samples (Kp2 peak on the left and kinks on the right). All the histograms are normalized to the number of events/incoming Kaons and have no energy threshold imposed. As can be seen in fig. 14, which is for sectors on the K path, the behaviour of the 3 samples is effectively the same in terms of K activity. The upper plots are the times with respect to tk, where an on-time peak at -0.6ns with 0.8ns sigma (from a Gaussian fit) is obvious, and the lower ones with respect to tpi, which show a decay lifetime shape. Fig. 15 shows the same distributions for sectors off the K path. In the lower plots (times with respect to tpi), a strong photon peak with 1.5ns sigma is present, at 2ns after tpi for the rejection samples only. A decay lifetime shape for the same samples is present in the upper plots (time with respect to tk). Fig. 16 and fig. 17 show the same for the CCDs, which have a similar mean, resolution and shift with respect to tpi.

The photon time distributions for Kp2 peak events and kinks are compared in fig. 18, where it can be seen that there is more photon activity in the AD for kinks. Comparing the number of events in the 3 bins of the photon peak for Kp2 peak and kinks, there is an approximate $18,900/11,000 = 72\%$ more activity in the kink sample measured by the TDCs and $28,000/17,500 = 60\%$ by the CCDs. In order to figure out if this excess is due to more hits per event or more events with more than 0 hits for kinks, off-path energy plots for peak and kinks were examined. About $310/1700 = 18\%$ of events have 0 energy for the Kp2 peak, and $82/608 = 13\%$ for kinks. The average number of AD hits per event is $4594/1700 \simeq 2.7$ for peak and $1770/608 \simeq 2.9$ for kinks. Therefore, the extra activity for kinks comes mostly from more events with more than 0 hits.

Time closest to tk/tpi vs total energy distributions for the same samples are shown in fig. 19 (fig. 20 for CCDs) and energy distributions for the 2 timing peaks in fig. 21 (fig. 22 for CCDs). The time selection (hit closest to tk or tpi) was just a logical way to assign one time per event, more representative than something like an average over all hits of the event (all the previous time plots are for every hit, therefore this bias is avoided). The K energy peak in time with tk is prominent for all samples, whereas most of the energy in time with tpi is at zero for the acceptance sample, and near zero with long high-energy tails for the rejection ones, as expected for showering photons.

In addition to the photon peak in fig. 15, some K activity remnants in time with tk are present, that are the same for all samples. These are due to the inefficiencies in calculating the K path mentioned earlier. To investigate further, fig. 23 shows the time distributions of the TDC and CCD hit closest to tk in every sector (same argument for time bias as in the previous paragraph stands here), for sectors on or off the Kaon path, for Km21's and Kp2 peak. The black and red histograms have the same number of events, but the "off path" ones have many more overflows, due to sectors with no activity at all, that have been ommitted for plotting purposes. The fraction of "on path" sectors that do not have a hit in time with tk (defined as within 4ns of tk) give the false sector assignment percentage. The fraction of "off path" sectors with a hit in time with tk give the inefficiency of the method. Multiplying these fractions with the average number of sectors on (off) the K path per event (see fig. 32 or 33 and accompanying text), we get the average number of sectors misassigned (missed) per event. The results are shown in table 4.

Therefore, the real number of sectors hit by the Kaon per event on average, corrected with the TDC and CCD F.A. and $\overline{\epsilon}$, is

$$\overline{N_{real}} = \overline{N^{onpath}_{meas.}} + \overline{N_{\overline{\epsilon}}} - \overline{N_{F.A.}}$$

	Km21		Kp2 peak			
	TDC	CCD	TDC	CCD	TDC	CCD
False assignment (F.A.)	18%	43%	20%	45%	0.583	1.313
Inefficiency ($\bar{\epsilon}$)	2.5%	4.4%	3.1%	4.8%	0.282	0.436

Table 4: The false sector assignment rate (number of sectors on the K path without a hit in time with tk over total number of sectors on the K path) and the inefficiency (number of sectors off the K path with a hit in time with tk over total number of sectors off the K path) of the K path finding algorithm, calculated from TDC and CCD data for Km21's and Kp2 peak. The last two columns are the Kp2 peak results scaled by the average number of sectors on the K path (2.917, see fig. 32) to give the false assignment per event, and by the average number of sectors off the K path (12-2.917) to give the inefficiency per event.

$$\begin{aligned} \overline{N_{real}^{TDC}} &= 2.917 + 0.282 - 0.583 = 2.616 \\ \overline{N_{real}^{CCD}} &= 2.917 + 0.436 - 1.313 = 2.040 \end{aligned} \qquad (1)$$

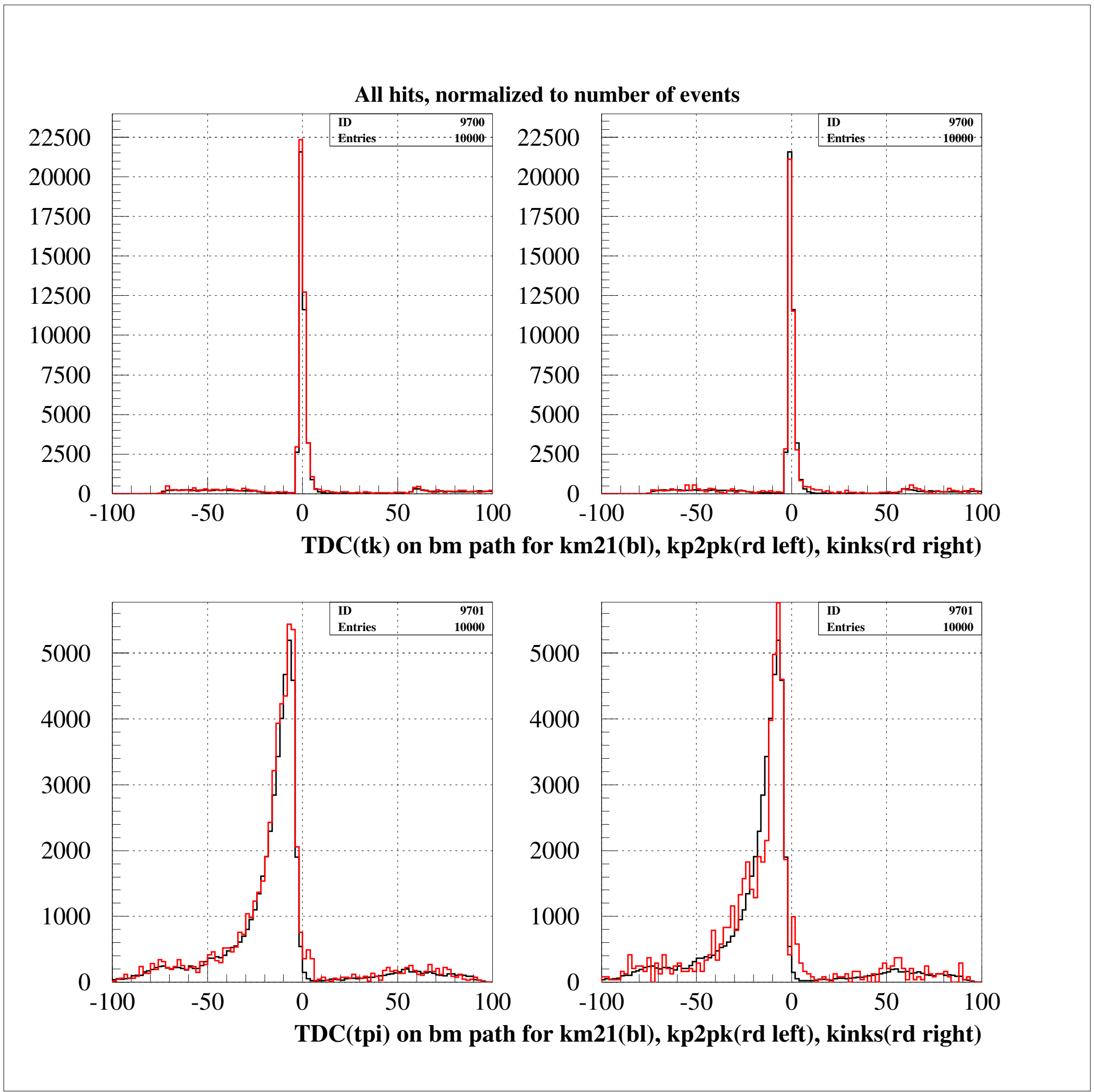

Figure 14: Time distributions of the TDC hits with respect to tk (top row) and tpi (bottom row) for sectors on the incoming Kaon path. Black histograms are for the acceptance sample (Km2 monitors) and red for the 2 rejection samples (Kp2peak on the left and kinks on the right). The units on the vertical axis are arbitrary.

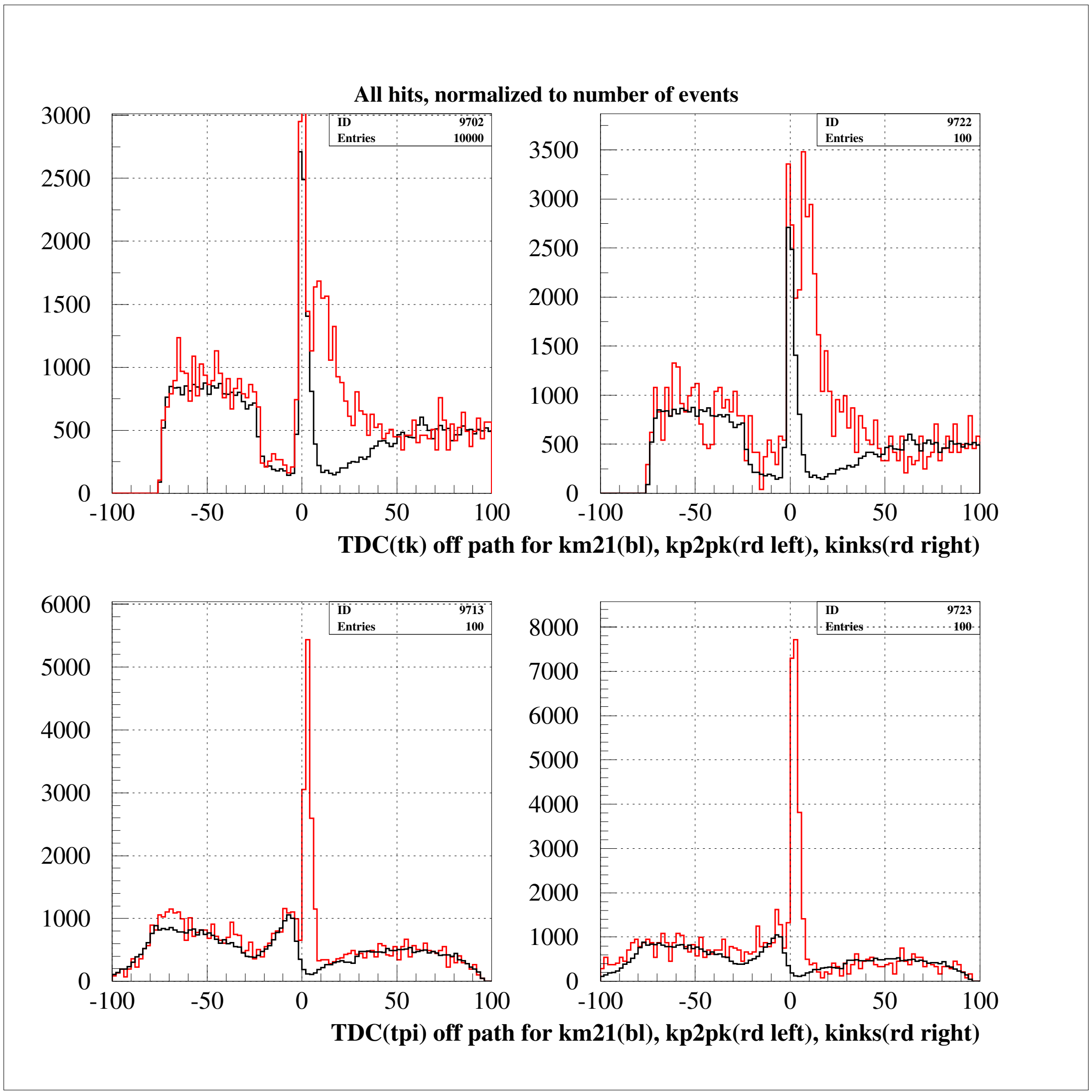

Figure 15: Time distributions of the TDC hits with respect to tk (top row) and tpi (bottom row) for sectors off the incoming Kaon path. Black histograms are for the acceptance sample (Km2 monitors) and red for the 2 rejection samples (Kp2peak on the left and kinks on the right). The units on the vertical axis are arbitrary.

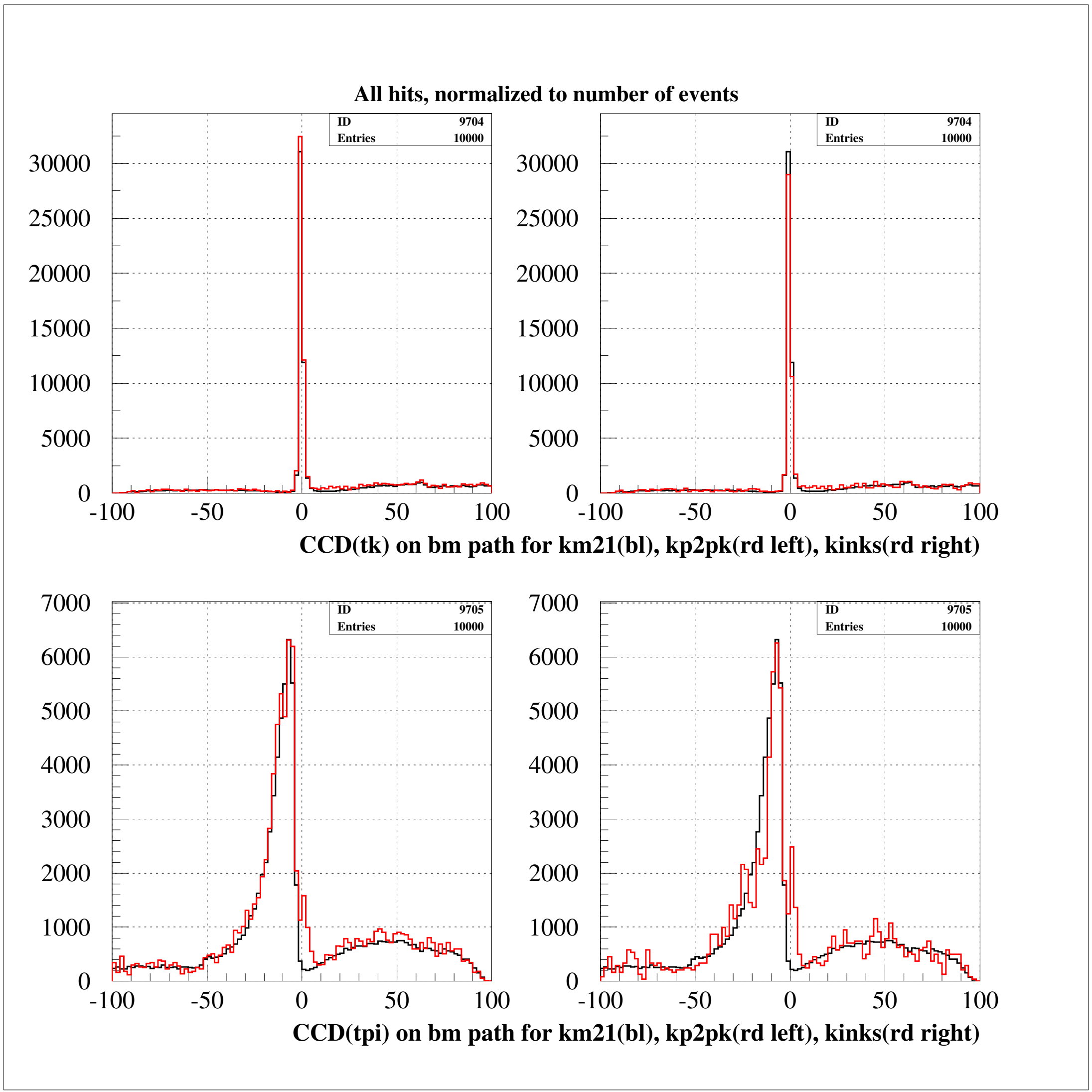

Figure 16: Time distributions of the CCD hits with respect to tk (top row) and tpi (bottom row) for sectors on the incoming Kaon path. Black histograms are for the acceptance sample (Km2 monitors) and red for the 2 rejection samples (Kp2peak on the left and kinks on the right). The units on the vertical axis are arbitrary.

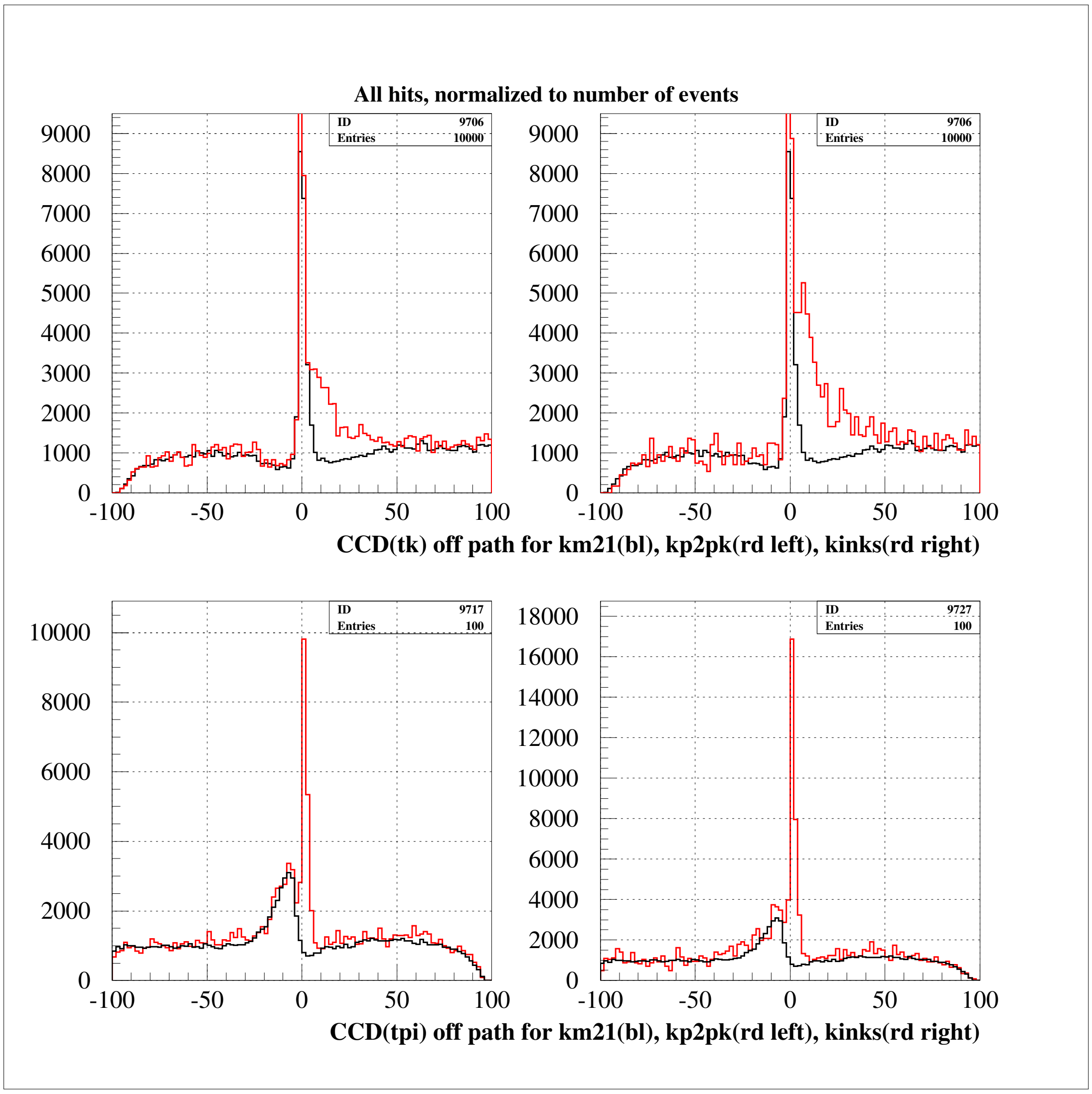

Figure 17: Time distributions of the CCD hits with respect to tk (top row) and tpi (bottom row) for sectors off the incoming Kaon path. Black histograms are for the acceptance sample (Km2 monitors) and red for the 2 rejection samples (Kp2peak on the left and kinks on the right). The units on the vertical axis are arbitrary.

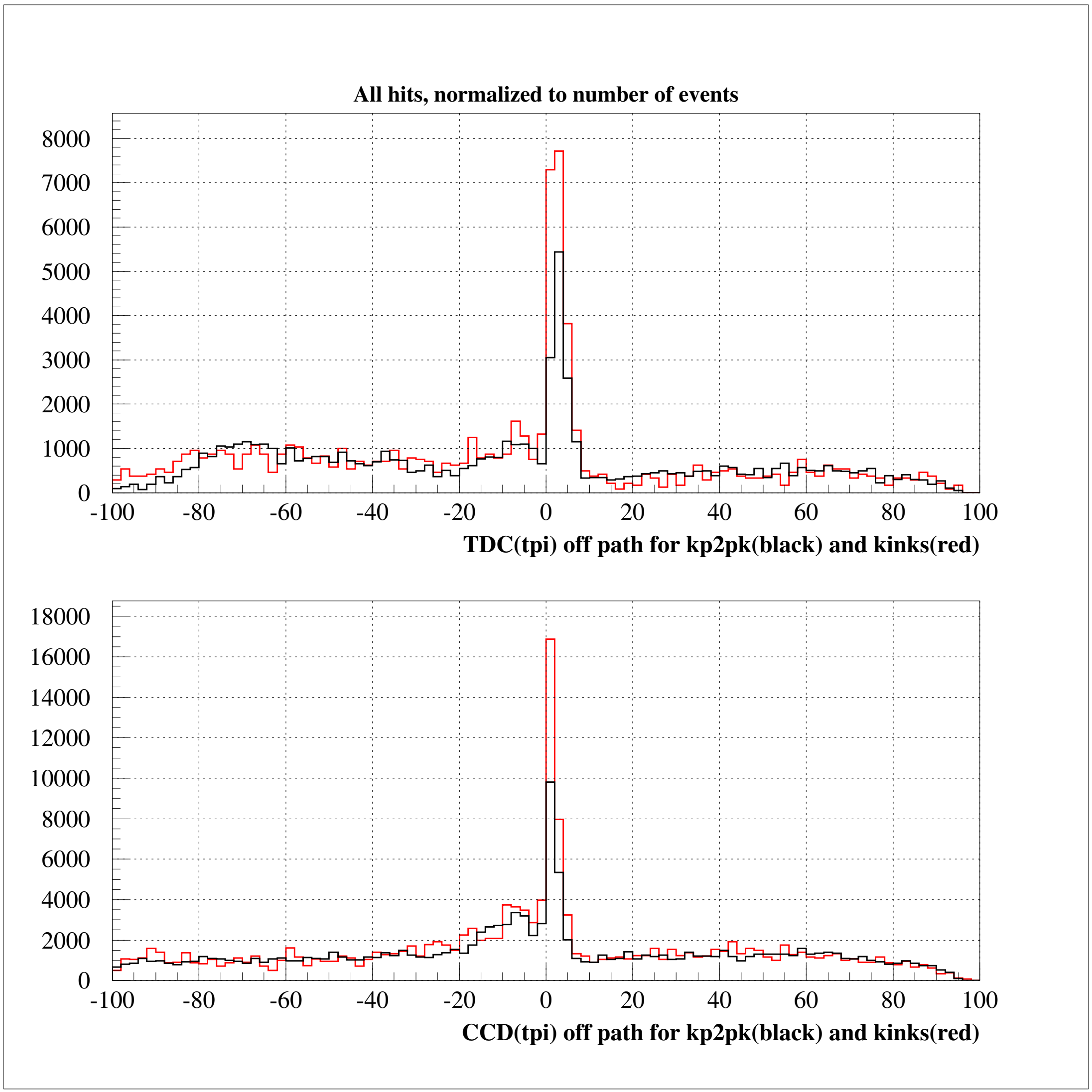

Figure 18: Time distributions with respect to tpi for sectors off the incoming Kaon path, from TDCs (top) and CCDs (bottom). Black histograms are for Kp2peak and red for kinks. The units on the vertical axis are arbitrary.

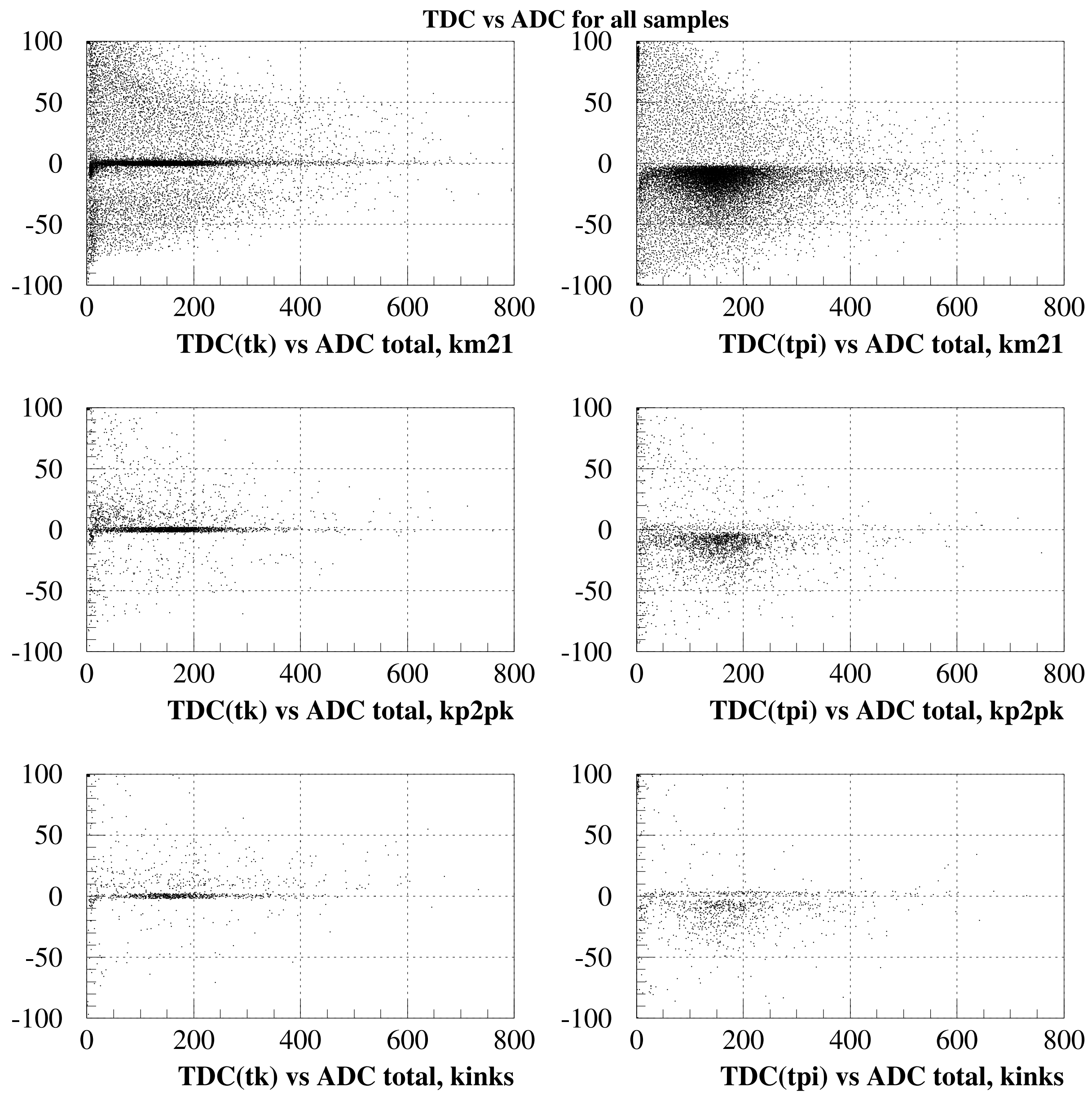

Figure 19: Time distributions with respect to tk (left) and tpi (right) of the TDC hit closest to tk or tpi, vs total ADC energy for Km21's (top), Kp2 peak (middle) and kinks (bottom).

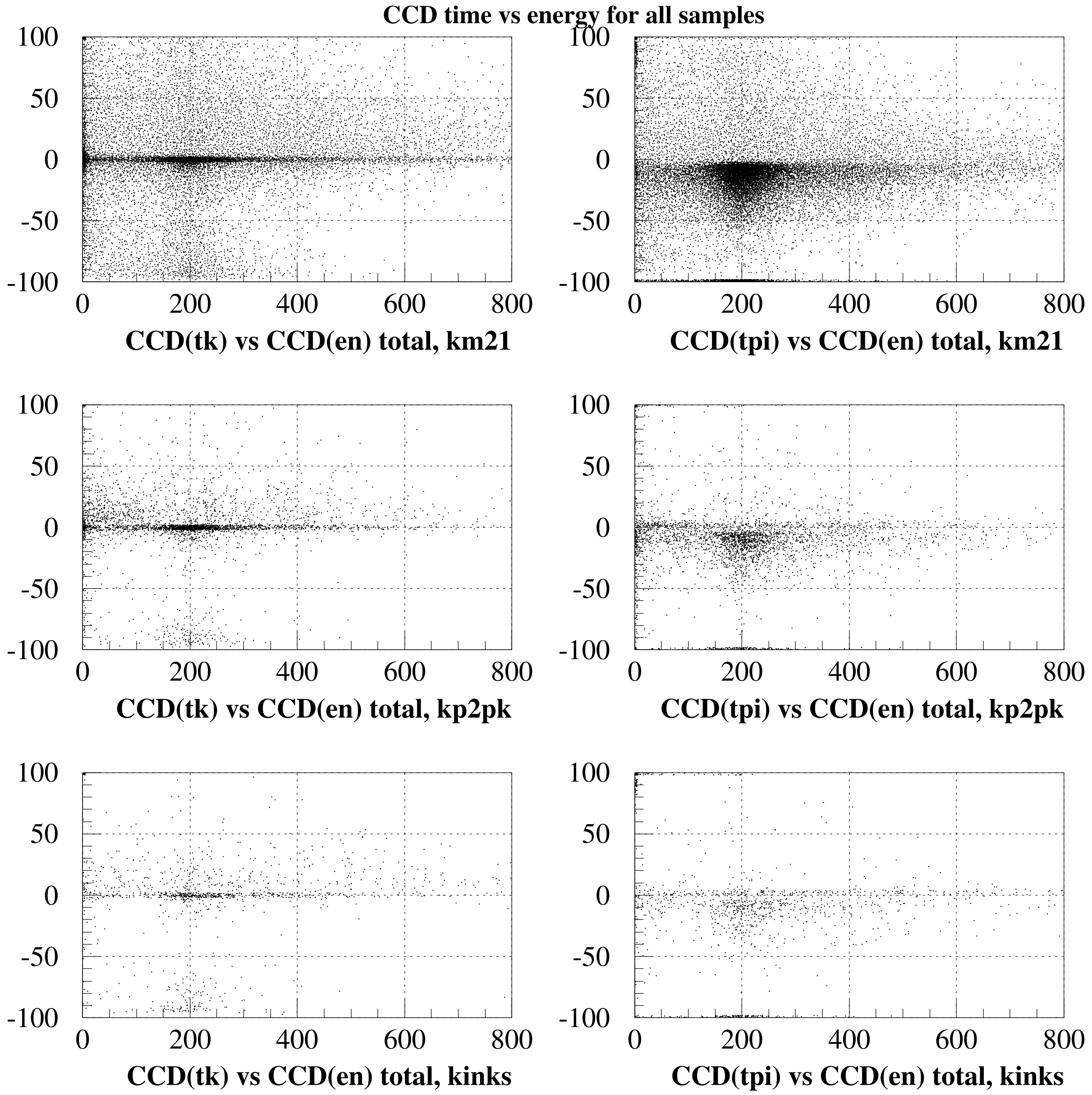

Figure 20: Time distributions with respect to tk (left) and tpi (right) of the CCD hit closest to tk or tpi, vs total CCD energy for Km21's (top), Kp2 peak (middle) and kinks (bottom).

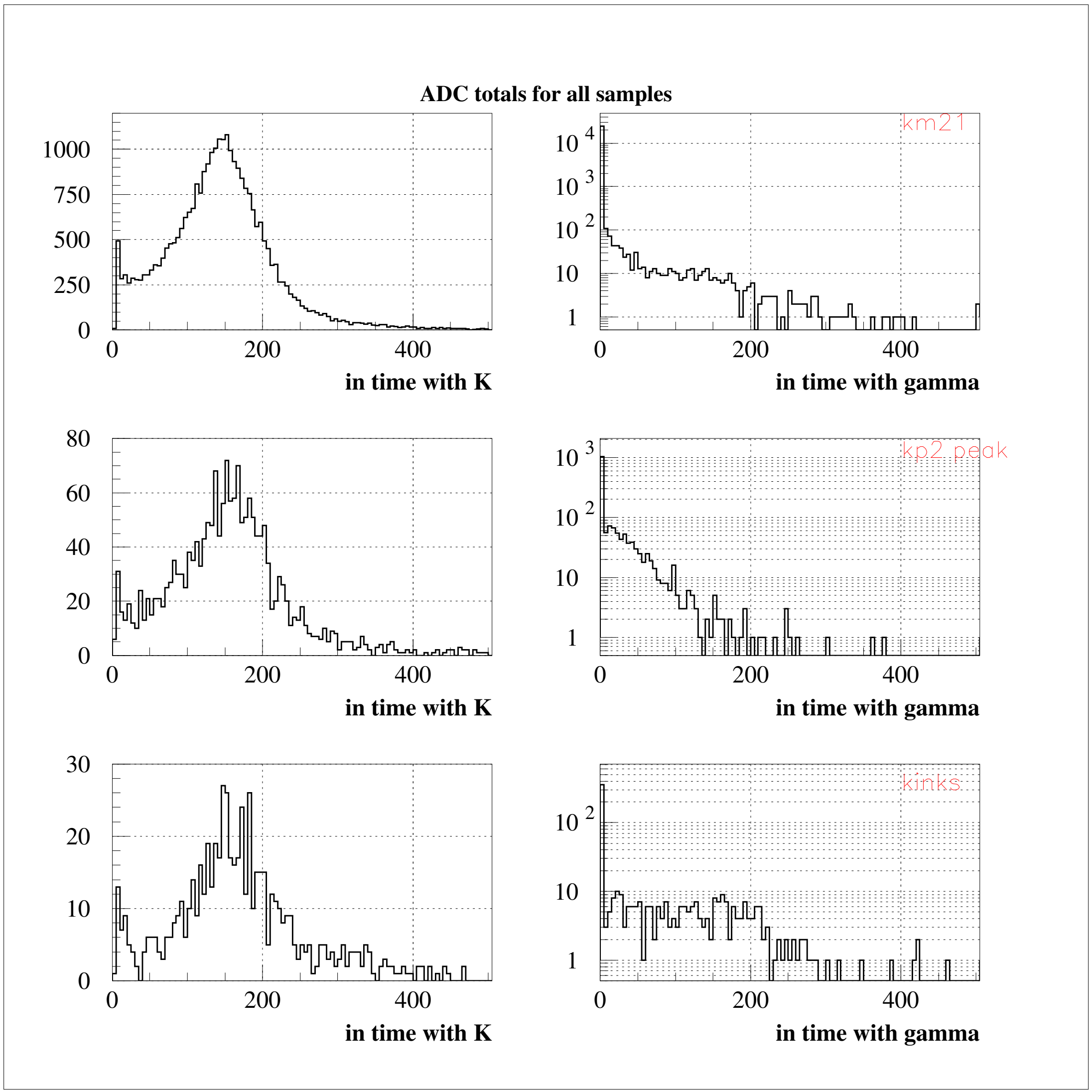

Figure 21: Total ADC energy in time with tk ($\pm 5ns$, left), and in time with the photon ($0 - 8ns$ from tpi, right) for Km21's (top), Kp2 peak (middle) and kinks (bottom).

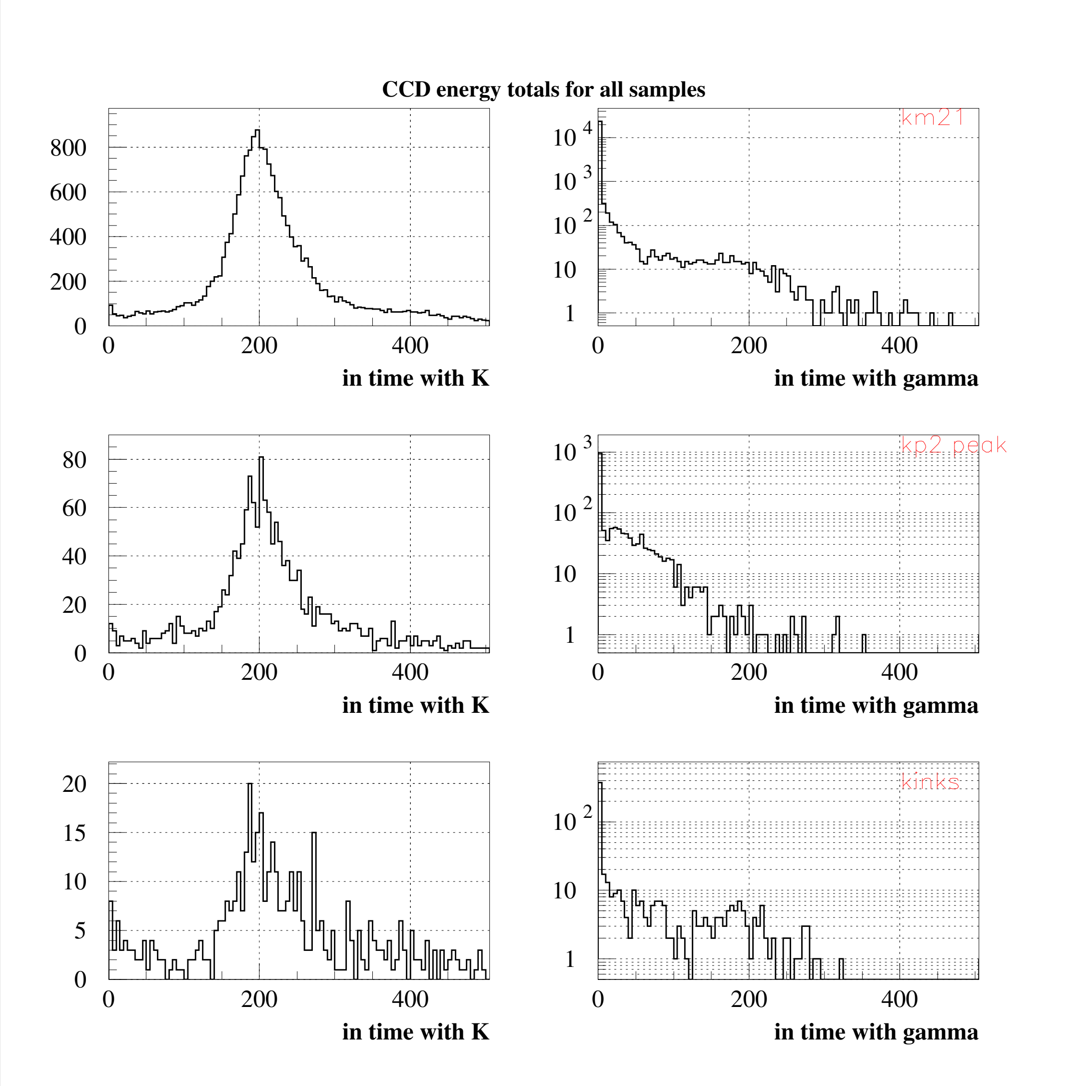

Figure 22: Total CCD energy in time with tk ($\pm 5ns$, left), and in time with tpi ($0-8ns$ from tpi, right) for Km21's (top), Kp2 peak (middle) and kinks (bottom).

5 Applying the cut

Based on the time and energy distributions in the AD, different ways to apply a PV cut were investigated. The main idea is to add the energy deposited either in whole sectors (for ADCs) or individual hits (for CCDs) and veto events based on this sum. For the ADCs, the different schemes are using sectors

- (a) with at least one TDC hit out of time with tk (>5ns) and in time with tpi (-2ns to 8ns)
- (b) same with (a) and no TDC hit at tk (±5ns)
- (c) same with (a) and the sector is also out of the K path

- (d) same with (b) and the sector is also out of the K path.

For the CCDs, hits are used that are either

- (a) in time with tpi and out of time with tk
- (b) same with (a) and in sectors out of the K path

The results, in the form of acceptance*rejection vs energy threshold, are shown in fig. 24 for the Kp2 peak and in fig. 25 for the kinks. For both the rejection samples, cutting on the sum of CCD “energy” at 5., irrespective of the sector the hit belongs to, seems to be the favorable case. The time window for this scheme was also optimized, as shown in fig. 26: the rej*acc for both rejection samples was measured for 24 different window settings, listed in table 5, and it was found to reach a plateau for a lower bound of -2ns, and not to change significantly for an upper bound above 8ns. The rejection, acceptance and rejection*acceptance for the lowest energy threshold for all cases are summarized in table 6.

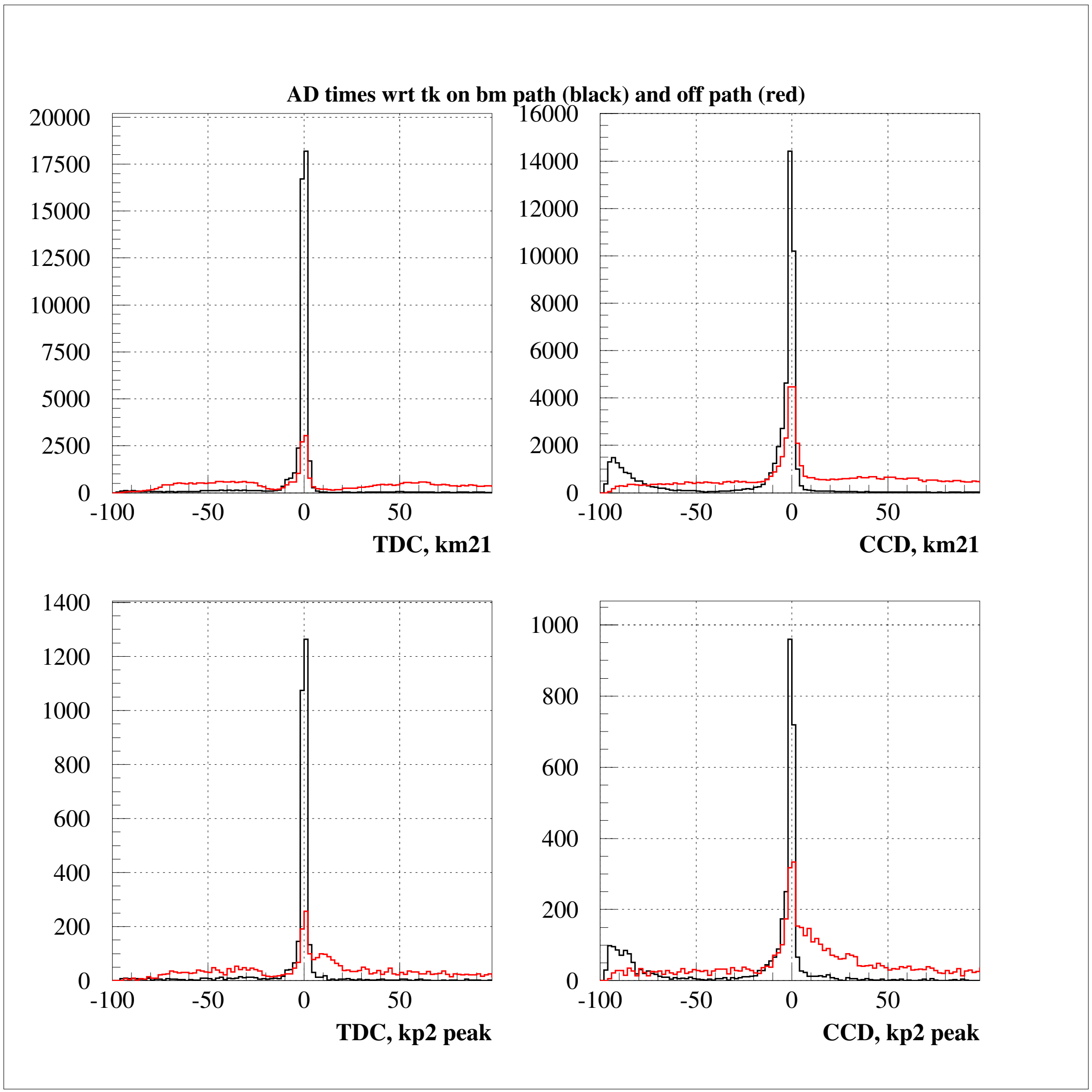

Figure 23: Time distributions with respect to tk of the TDC (left) and CCD (right) hit closest to tk in every sector, for sectors on (black) and off (red) the incoming Kaon path. The top row is for Km21's and the bottom row for Kp2 peak.

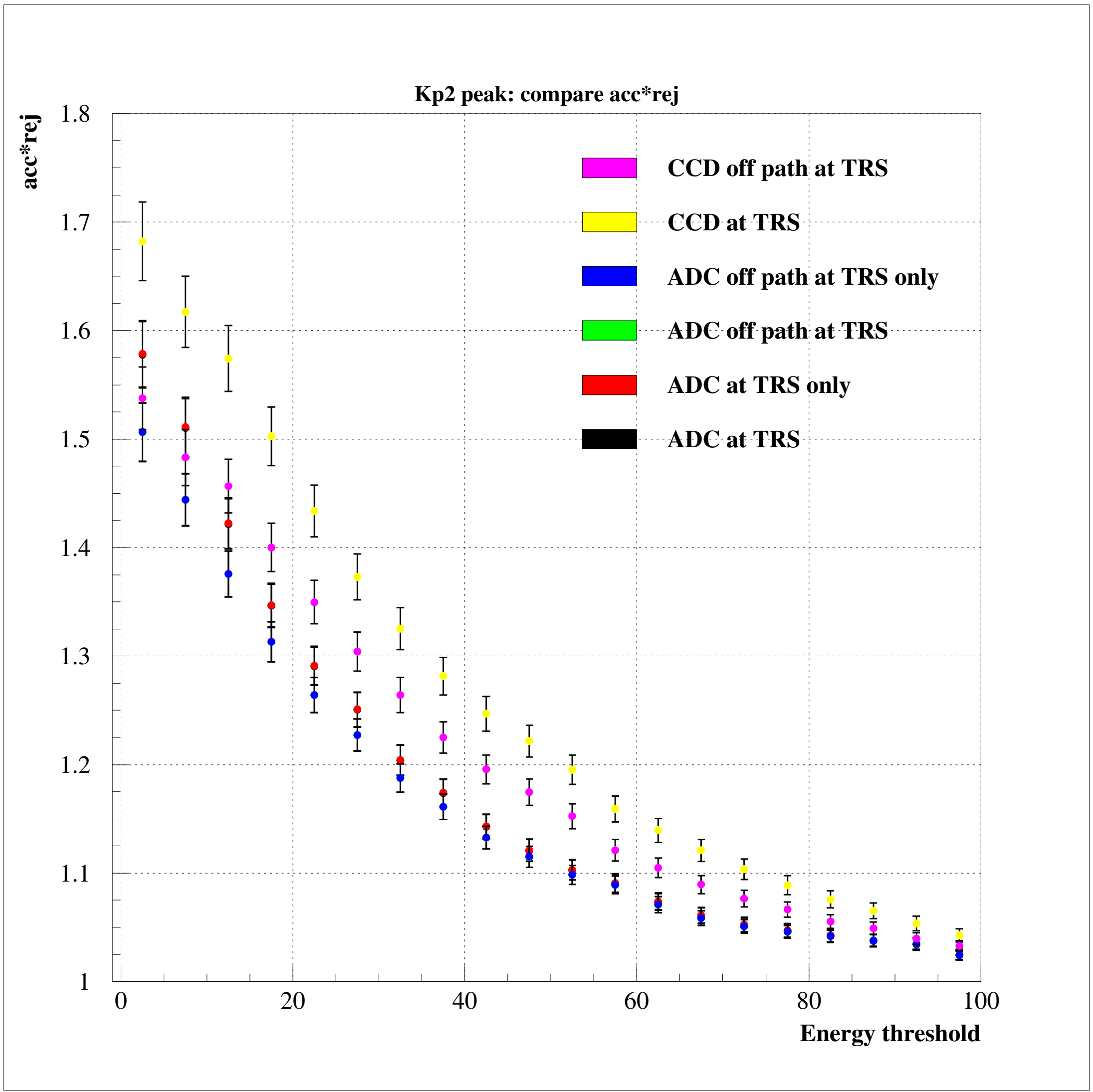

Figure 24: Acceptance*rejection vs total ADC or CCD energy threshold, for different sector selection, for Kp2 peak events. The different sets of points correspond to ADC cases a-d and CCD cases a-b explained in the text, from bottom to top. The points for ADC cases a and b (black and red), as well as c and d (green and blue), completely overlap.

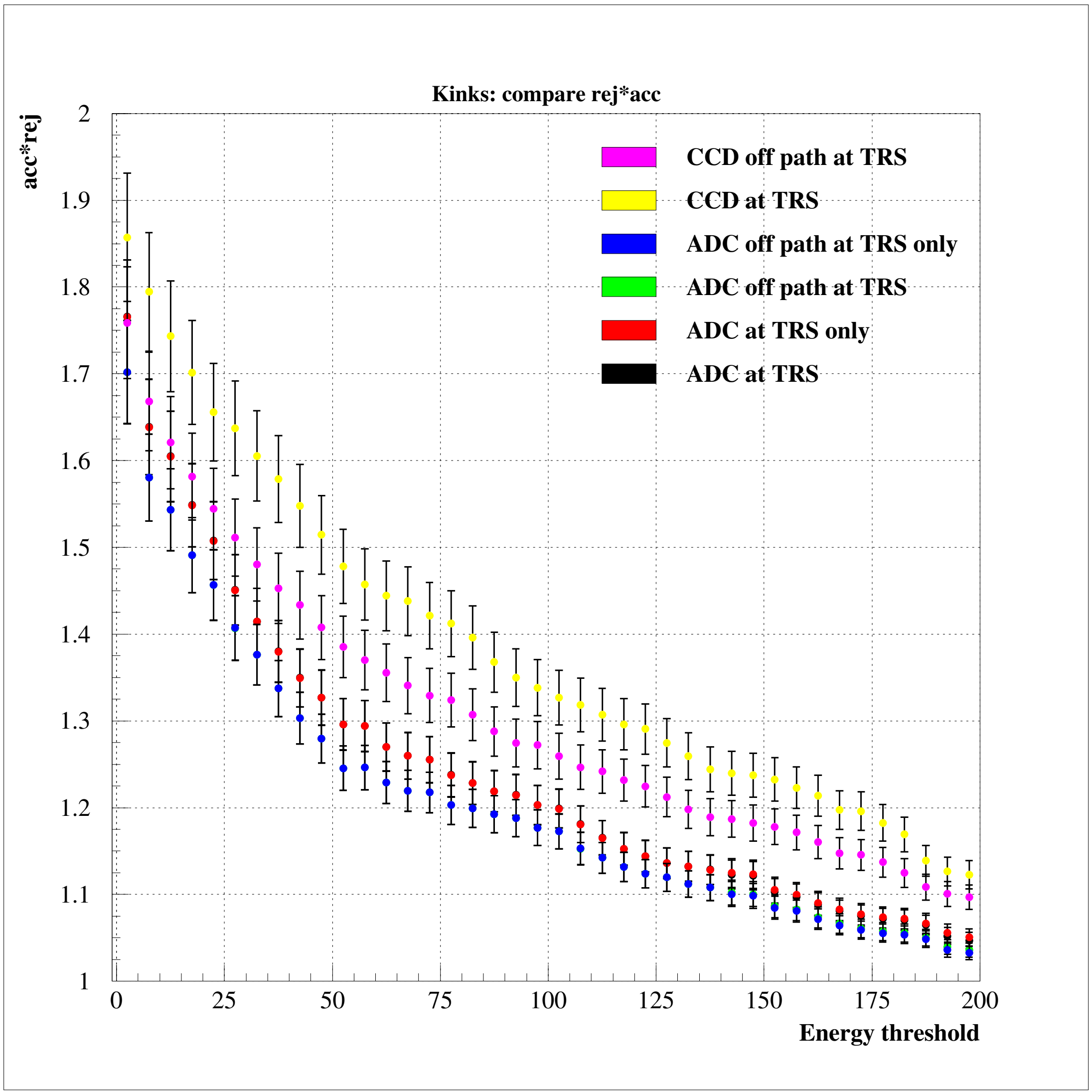

Figure 25: Acceptance*rejection vs total ADC or CCD energy threshold, for different sector selection, for kink events. The different sets of points correspond to ADC cases a-d and CCD cases a-b explained in the text, from bottom to top. The points for ADC cases a and b (black and red), as well as c and d (green and blue), completely overlap.

The same plots of rej*acc vs energy threshold for tighter setup PV cuts (at 53% acceptance) are shown for the Kp2 peak in fig. 27. Fig. 28 is for only the US EC inner ring (EC1) PV tightened. In both cases, the kink sample runs out of statistics for such tight PV level. The results for the optimal case (CCD (a), at the lowest threshold) are summarized in table 7. The rej*acc is a bit higher for the tight PV sample, and a bit smaller for the only-EC1 one, as expected for these two correlated subsystems (AD and EC1, see. [1]). In both cases, it follows the same trend as a function of energy threshold as the loose-PV case.

Further evidence of the AD-EC1 correlation is shown in fig. 29-31. The fraction of events with zero energy deposit in the EC1, remaining US EC and DS EC is shown as a function of the AD energy deposit for the 3 samples. The rest of the PV has not been applied on the rejection samples,

	t min (ns)	t max (ns)
1	-4	10
2	-3	10
3	-2	10
4	-1	10
5	0	10
6	-4	9
7	-3	9
8	-2	9
9	-1	9
10	0	9
11	-4	8
12	-3	8
13	-2	8
14	-1	8
15	0	8
16	-4	7
17	-3	7
18	-2	7
19	-1	7
10	0	7
21	-4	6
22	-3	6
23	-2	6
24	-1	6

Table 5: The time window settings used for fig. 26.

to increase statistics. From the Km2 sample, it can be seen that the accidentals rate is at about 10% for all pieces of the EC.

The rejection samples show a clear correlation between both US EC parts and the AD: 75% of the events with zero energy deposited in the AD have no energy in EC1, which drops to about 63% for even minimal AD energy, and continues to drop down to a minimum of about 40% for higher energies for the Kp2 peak sample. In the rest of the US EC, the corresponding percentages are 65%, 62% and a plateau of about 50%. For the kink sample, 70% of the events with zero energy deposited in the AD have no energy in EC1, which drops to about 53% for even minimal AD energy, and continues to drop down to a plateau of about 15% for higher energies. The respective percentages for the rest of the US EC are 57%, 53% and 25%. The rise of these numbers in both the rejection samples for very high AD energies, is due to the online PV that has already cut events with high energy deposits in the EC. These events most likely also leave the highest energy in the AD.

For the DS EC, both the rejection samples show an anti-correlation, with 55% of the events with zero AD energy having no energy in the DS EC for the Kp2 peak and 42% for the kink sample. For the Kp2 peak sample, this value rises to a peak of about 85% and then drops to a plateau of about 60%, whereas for the kinks, it quickly reaches a plateau of 55%, as the energy deposit in the AD

	ADC (a),(b)	ADC (c),(d)	CCD (a)	CCD (b)
acc	0.96±0.001	0.98±0.001	0.94±0.002	0.97±0.001
Kp2 peak				
rej	1.64±0.03	1.54±0.03	1.79±0.04	1.59±0.03
acc*rej	1.58±0.03	1.51±0.02	1.68±0.04	1.54±0.03
Kinks				
rej	1.81±0.07	1.73±0.05	1.95±0.08	1.80±0.07
acc*rej	1.76±0.08	1.70±0.06	1.86±0.08	1.76±0.08

Table 6: Rejection, acceptance and rej*acc of different implementations of the AD photon veto for both rejection samples, for the lowest thereshold (5.).

	loose PV (95%)	tight PV (53%)	tight EC1
acc	0.94±0.002	0.95±0.002	0.95±0.002
rej	1.79±0.04	1.95±0.14	1.69±0.07
acc*rej	1.68±0.04	1.86±0.13	1.60±0.06
EC1 parameters			
t half-window	2 ns	5.15 ns	5.15 ns
E threshold	2 MeV	0.2 MeV	0.2 MeV

Table 7: Rejection, acceptance and rej*acc of CCD(a) for the lowest thereshold (see text) for different setup PV cut, for Kp2 peak. The EC1 veto parameters for every setting are given.

increases. These results are summarized in table 8

Subsystem	Zero AD energy	Minimal AD energy	Higher AD energy
		Km2 (100% - accidentals rate)	
EC1	88%	88%	88%
US EC	91%	91%	91%
DS EC	87%	89%	89%
		Kp2 peak	
EC1	75%	63%	minimum of 40%
US EC	65%	62%	drops to plateau of 50%
DS EC	55%	62%	maximum of 85%, then plateau of 60%
		Kinks	
EC1	70%	53%	drops to plateau of 15%
US EC	57%	53%	drops to plateau of 25%
DS EC	42%	47%	up to plateau of 55%

Table 8: Percentage of events with zero energy deposit in different parts of the EC for different energy deposits in the AD, for all the samples. The numbers are read off fig. 29-31.

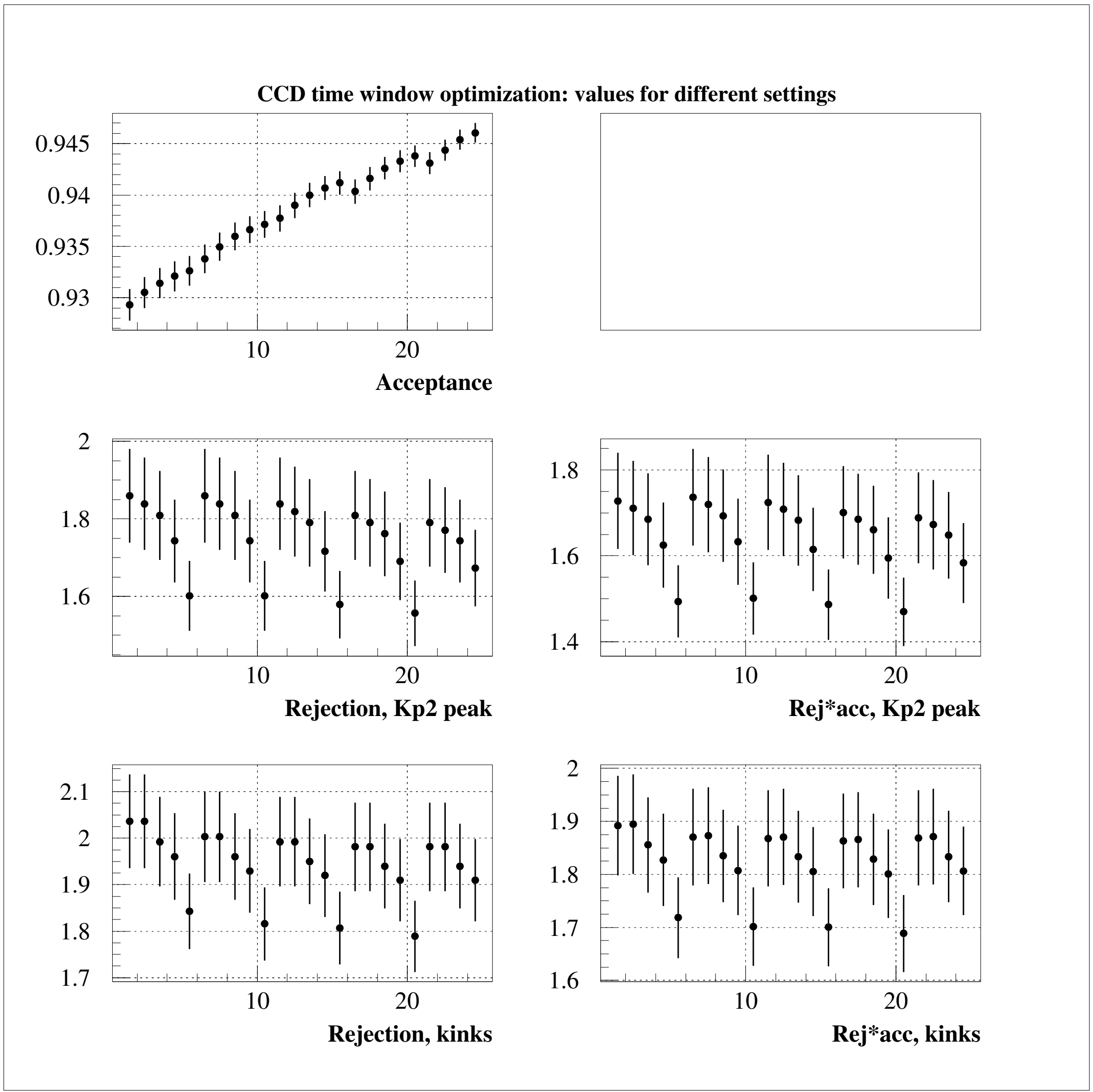

Figure 26: Acceptance, rejection and acc*rej for different time windows, listed in table 5. The CCD thereshold (scheme (a)) is at 5.

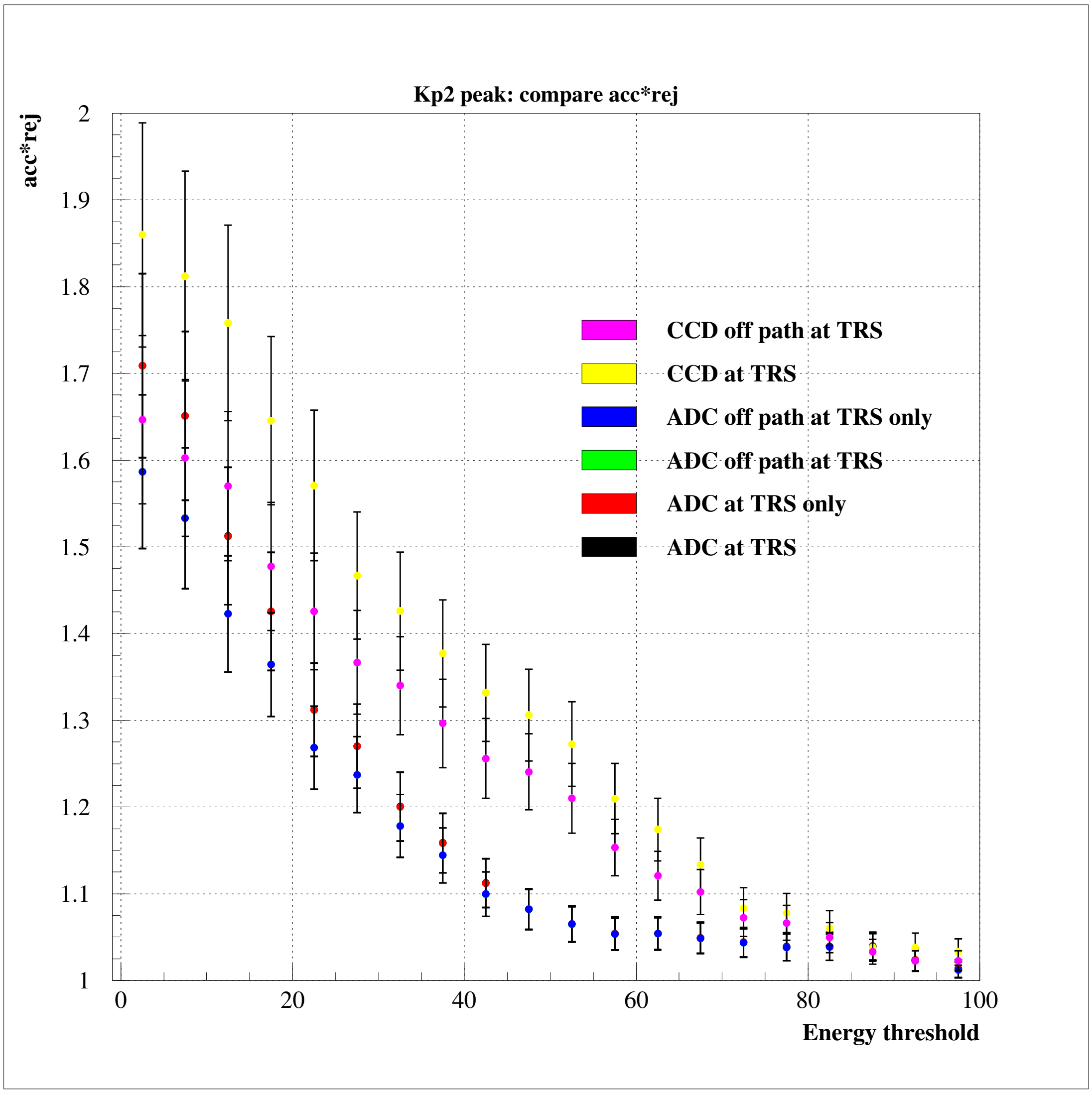

Figure 27: Acceptance*rejection vs total ADC or CCD energy threshold, for different sector selection, for Kp2 peak events with tight setup PV. The different sets of points correspond to ADC cases a-d and CCD cases a-b explained in the text, from bottom to top. The points for ADC cases a and b (black and red), as well as c and d (green and blue), completely overlap.

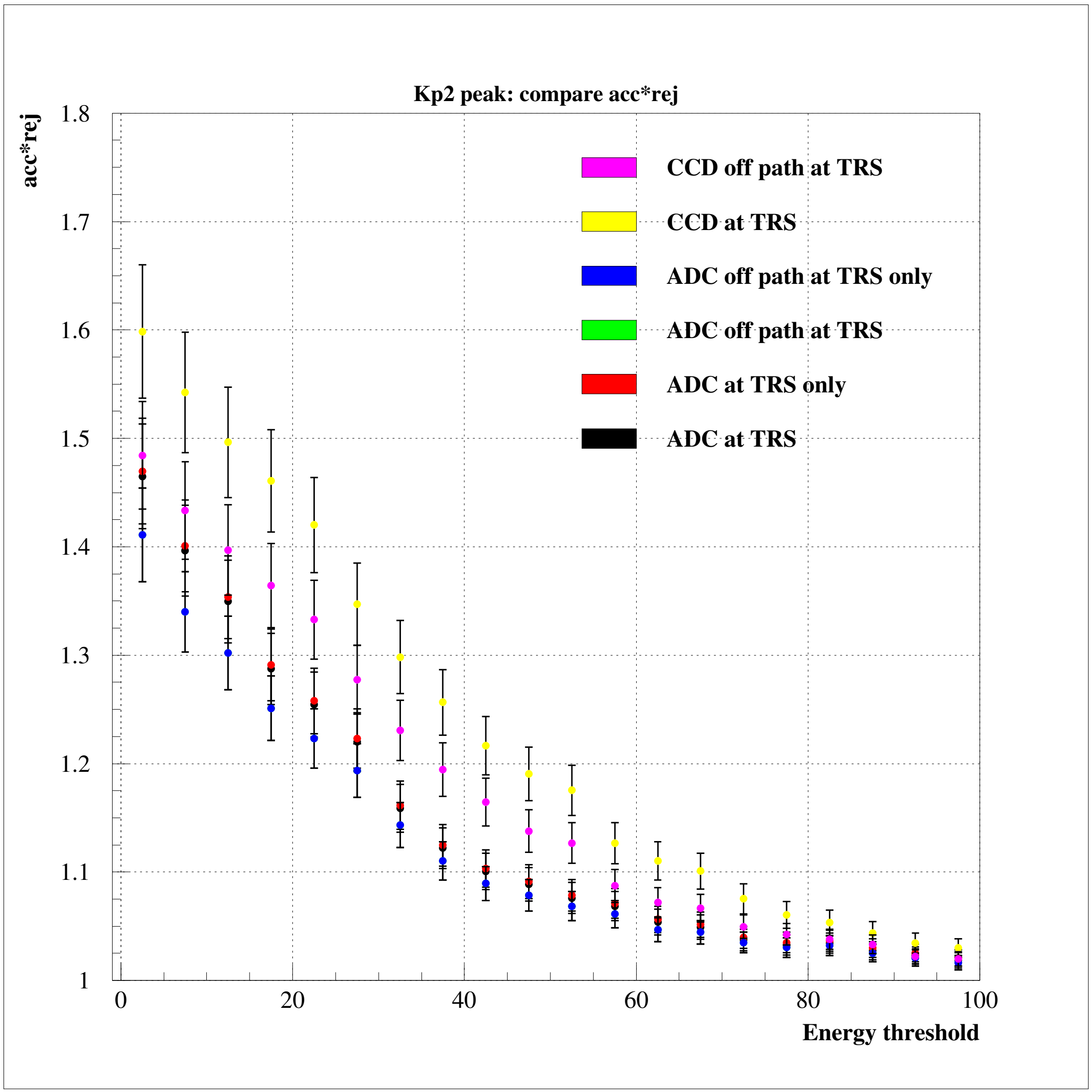

Figure 28: Acceptance*rejection vs total ADC or CCD energy threshold, for different sector selection, for Kp2 peak events with tight setup US EC inner ring PV, with the rest of the systems at a loose setting. The different sets of points correspond to ADC cases a-d and CCD cases a-b explained in the text, from bottom to top. The points for ADC cases a and b (black and red), as well as c and d (green and blue), completely overlap.

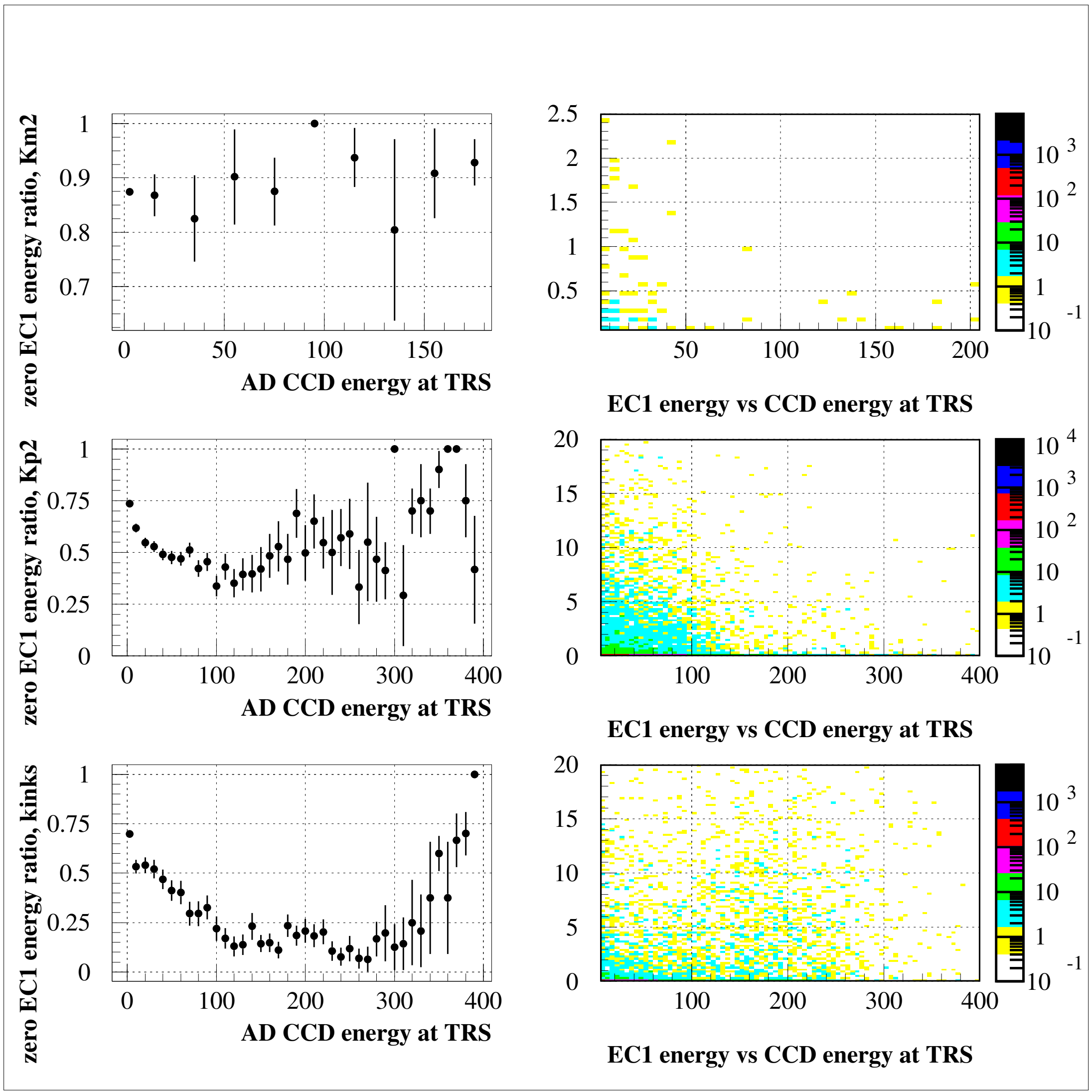

Figure 29: Percentage of events with zero energy deposit in the EC1 as a function of energy deposit in the AD (left) and the scatter plots of EC1 energy vs AD CCD energy that these graphs were created from (right), for Km21's (top), Kp2 peak (middle) and kinks (bottom).

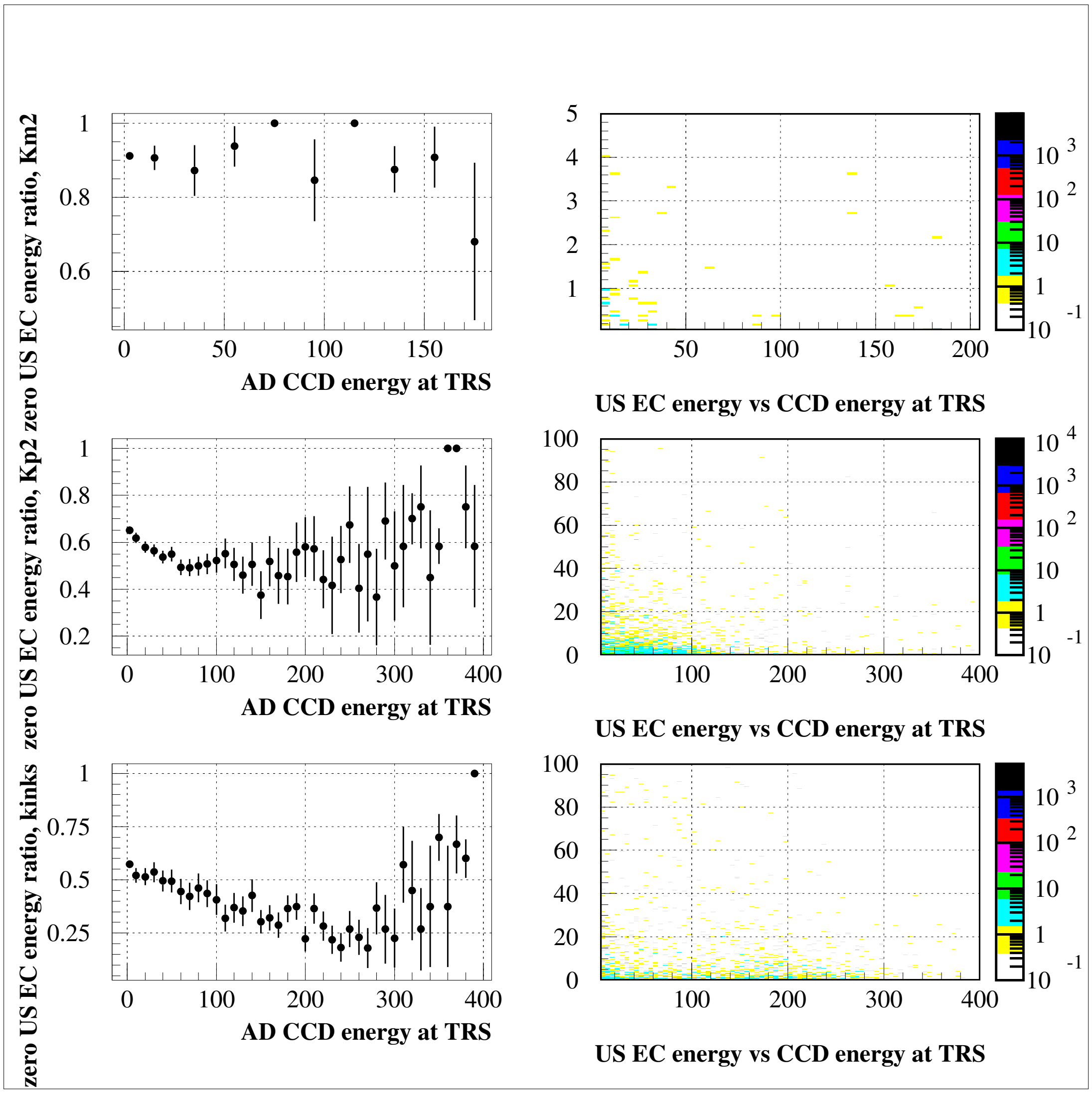

Figure 30: Percentage of events with zero energy deposit in the US EC (without the inner ring) as a function of energy deposit in the AD (left) and the scatter plots of EC1 energy vs AD CCD energy that these graphs were created from (right), for Km21's (top), Kp2 peak (middle) and kinks (bottom).

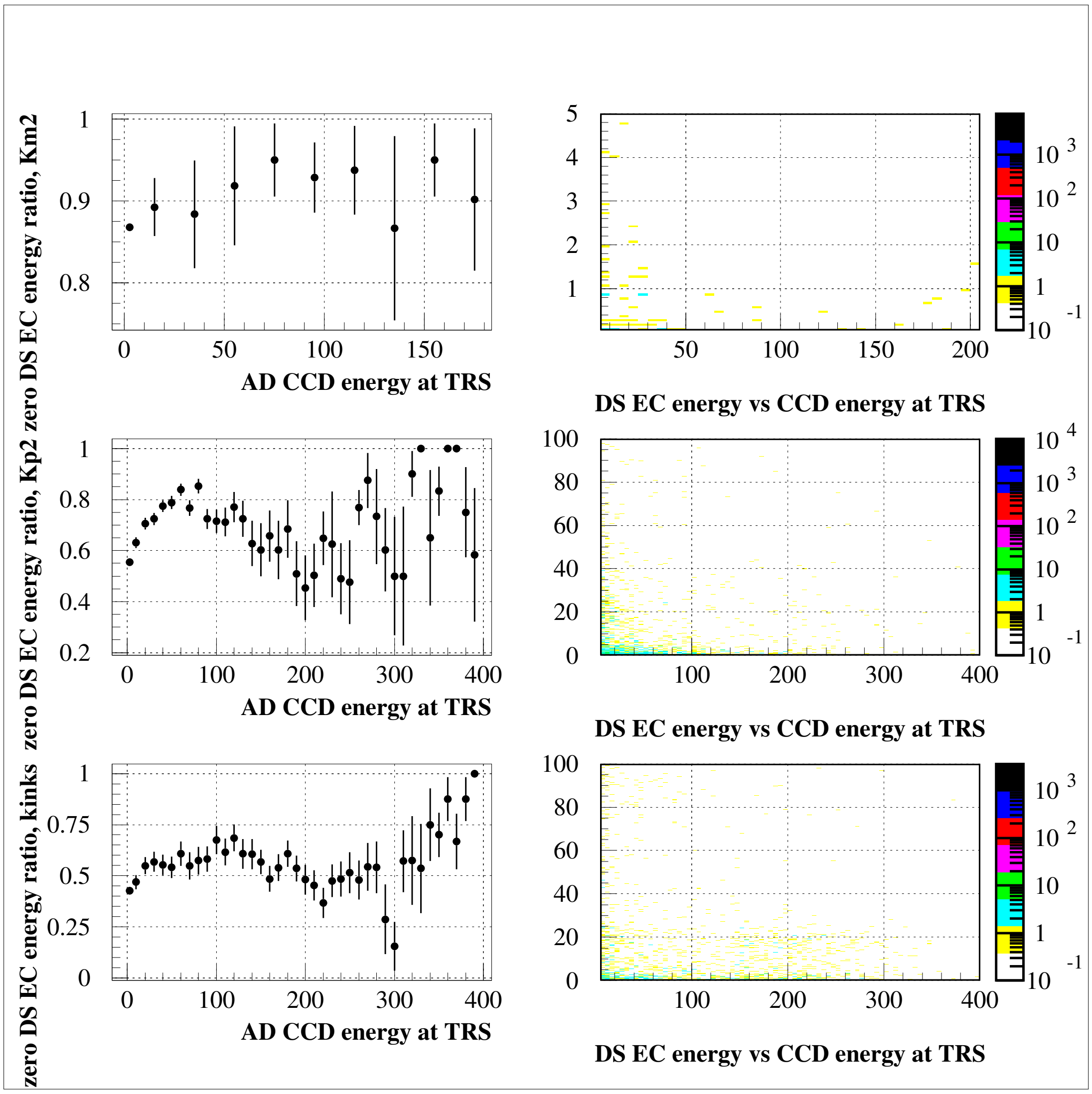

Figure 31: Percentage of events with zero energy deposit in the DS EC as a function of energy deposit in the AD (left) and the scatter plots of EC1 energy vs AD CCD energy that these graphs were created from (right), for Km21's (top), Kp2 peak (middle) and kinks (bottom).

The rej*acc graphs also shed light on the question of how much photon activity is hidden under the Kaon sectors and how efficiently we can veto on it (losing the least acceptance) by using CCD pulse fits. It is evident that even if we veto on *any* activity at tpi in K sectors, the acceptance loss is offseted by the rejection gain (the acc*rej remains about the same, if not slightly higher). More detail is available in fig. 32 and fig. 33, which show the multiplicity (number of sectors hit) of the K, based on its extrapolated track and its timing, as well as the photon at TRS for KP2 peak events. 2.567 sectors on average have TDC hits at tk and 1.748 at trs (whenever there is some energy deposit at photon time, therefore the zero bin is not included in the average). The CCDs give 3.496 and 2.182 respectively, and the path-extrapolating algorithm gives 2.917 sectors hit by the Kaon on average.

The number of sectors on the K path that have also non-zero energy hits at TRS is also shown, by itself and as a function of the total number of sectors with non-zero hits at TRS. 4.37% of the events have non-zero energy hits at TRS in sectors on the K path according to the TDCs, and 11.7% according to the CCDs. These numbers have to be corrected for the false assignments and the inefficiencies of the path-finding algorithm, by the ratio of the real number of sectors hit by the Kaon per event (see equation 1), over the measured average by the TDCs ($f_{TDC} = \frac{2.616}{2.567} = 1.019$) and CCDs ($f_{CCD} = \frac{2.040}{3.496} = 0.584$).

Finally, the energy deposited in all sectors at TRS vs the energy only in the ones transversed by the Kaon is plotted. It turns out, from the number of events in the diagonal of the 2 last plots, which are the ones that all the photon activity is hidden under the Kaon, that, from the events that have photon energy hidden under the K sectors, 74.32% do not have significant ADC energy outside these sectors to veto on and 60.61% do not have CCD energy outside these sectors. Therefore, at most $0.0445 \times 0.7432 = 3.31\%$ more events could be vetoed using second-pulse information, and some of this potential is used by the simple pulse-finding of the CCDs without losing significant acceptance (see table 6: the rejection of the CCD scheme (a) is about 8-9% more than the rejection of the ADC scheme (a)) This information is summarized in table 9.

	# of events	fraction of total
with TDC hits at TRS on beam path sectors	$\frac{74}{1693} \times f_{TDC} = 4.45\%$	4.45%
with TDC hits ONLY on beam path sectors at TRS	55/74=74.32%	3.31%
with CCD hits at TRS on beam path sectors	$\frac{198}{1693} \times f_{CCD} = 6.83\%$	6.83%
with CCD hits ONLY on beam path sectors at TRS	120/198=60.61%	4.14%

Table 9: Numbers of events with photon activity under the Kaon sectors. The numbers come from projections of the plots in fig. 32 and 33.

As a final check, the AD CCD scheme (a) rejection as a function of DELCO is shown in fig. 34. The Kp2 peak distribution is depleted for low DELCO due to the effect of CCDPUL, whose acceptance loss is higher in this region (CCDPUL, as well as some other TGCUTS, has not been applied on the kink sample, in order to retain statistics). Although there is a small (about 10%) gain in AD rejection according to these plots for DELCO>5ns, it is not significant enough to pursue the use of CCD pulse fits. In principle, the CCD pulse finding and fitting should give the same results for high DELCO.

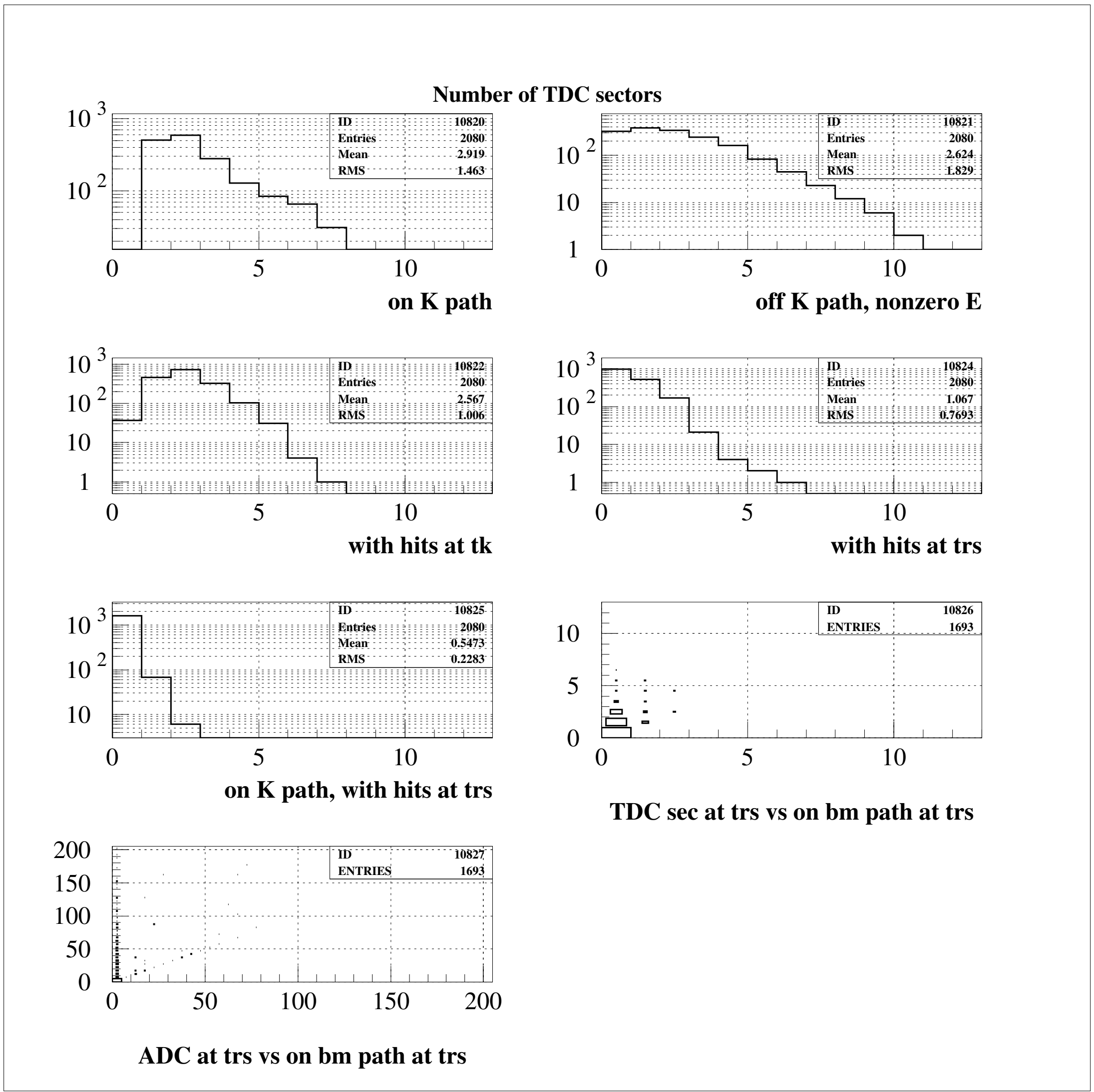

Figure 32: Number of sectors hit by incoming Kaons and outgoing photons for Kp2 peak: (a) on the extrapolated K path (b) off the extrapolated K path with non-zero ADC energy deposit (c) with TDC hits in time with tk (d) with TDC hits in time with TRS (e) with TDC hits in time with TRS on the extrapolated K path (f) number of sectors with TDC hits in time with TRS vs number of sectors with TDC hits in time with TRS on the extrapolated K path (g) total ADC energy deposited at sectors with hits at TRS vs total ADC energy deposited at sectors with hits at TRS on the K path.

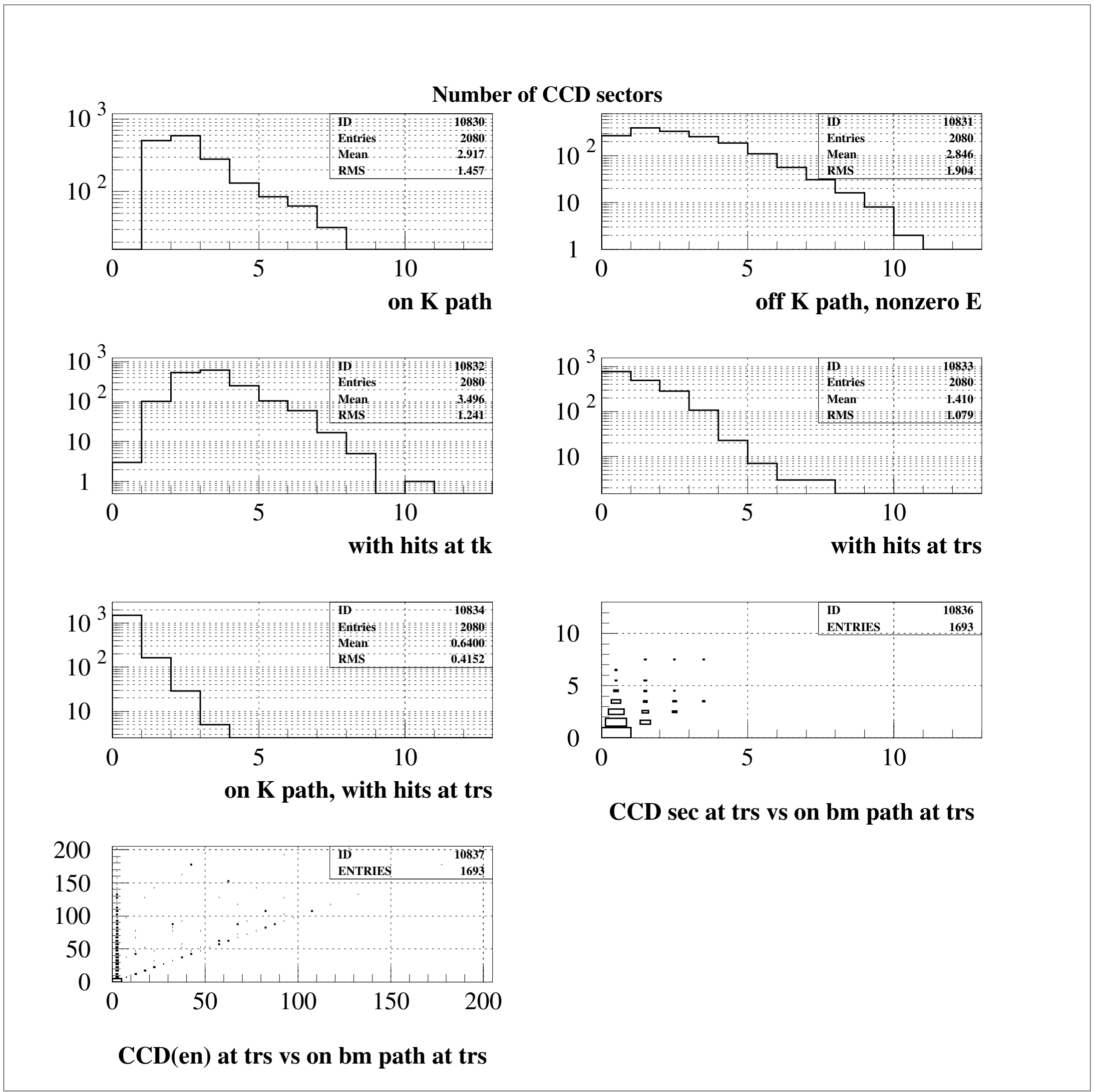

Figure 33: Number of sectors hit by incoming Kaons and outgoing photons for Kp2 peak: (a) on the extrapolated K path (b) off the extrapolated K path with non-zero CCD energy deposit (c) with CCD hits in time with tk (d) with CCD hits in time with TRS (e) with CCD hits in time with TRS on the extrapolated K path (f) number of sectors with CCD hits in time with TRS vs number of sectors with CCD hits in time with TRS on the extrapolated K path (g) total CCD energy deposited at sectors with hits at TRS vs total CCD energy deposited at sectors with hits at TRS on the K path.

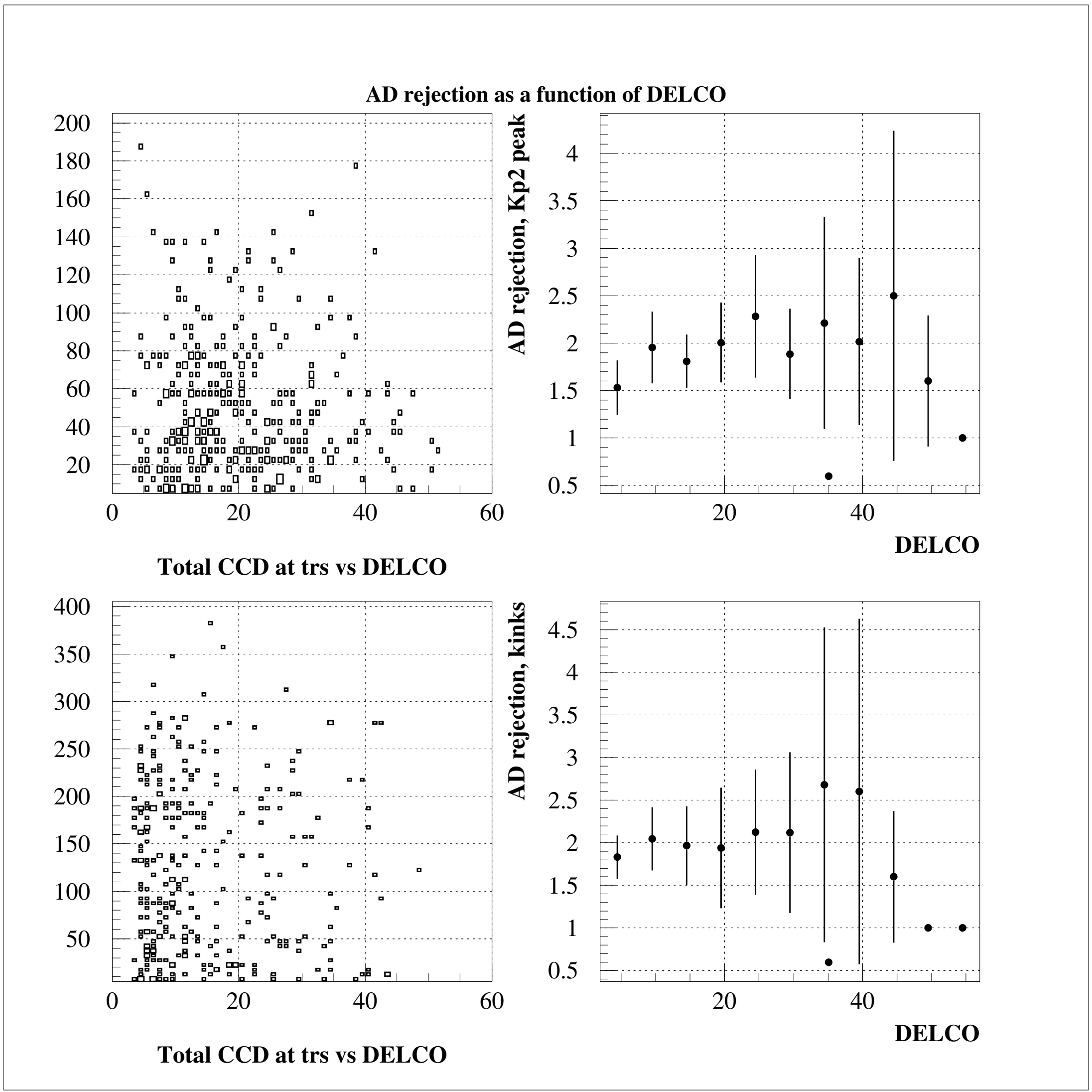

Figure 34: Total AD CCD energy at TRS scatter plots (left) and AD rejection (number of events in every 5ns DELCO bin over number of zero energy events in that bin) vs DELCO (right) for Kp2 peak events (upper) and kinks. The zero energy bin has been cut off for plotting purposes in the scatter plots. The lone point at 35ns and 0.5 rejection in the rejection plots should be ignored.

The AD rejection power was also investigated with tighter setup PV cuts. The offline rejection vs offline acceptance for different tightness for all PV subsystems, with the AD contribution at the optimal cut configuration (as explained in the previous paragraph) is shown in fig. 35 for the Kp2 peak and fig. 36 for 6 different classes of events in the PNN2 box. The setup cuts for these SKIM5 event classes are the same as the ones for the Kp2 peak sample (apart from the BOX cut, of course), except for the TGCUTS, which are selectively inverted to pick different samples of Kp2 scatters in the target, similar to events that are identified as kinks in SKIM8. Table 10 lists these class selection cuts. As it can be seen in these plots, the AD still has rejection power when the other PV subsystems are tightened. It especially contributes to the rejection in the middle range of acceptances (40%-55%), where the EC1 has been found to be inefficient (optimization under way).

CLASS	TGCUTS
3	$\overline{CCDPUL}$
6	CCDPUL, TGZFOOL, EIC, OPSVETO, $\overline{OTHERS}$
8	$\overline{CCDPUL}$,$\overline{CHI567}$,$\overline{VERRNG}$
11	$\overline{CHI567}$,$\overline{VERRNG}$
14	$\overline{CCDPUL}$,$\overline{CHI567}$,$\overline{VERRNG}$,KIC,PIGAP,TARGF,TPICS
15	$\overline{B4EKZ}$

Table 10: Classes of events used to measure the PV and AD rejection in the PNN2 box. All the setup cuts previously mentioned were applied to all classes.

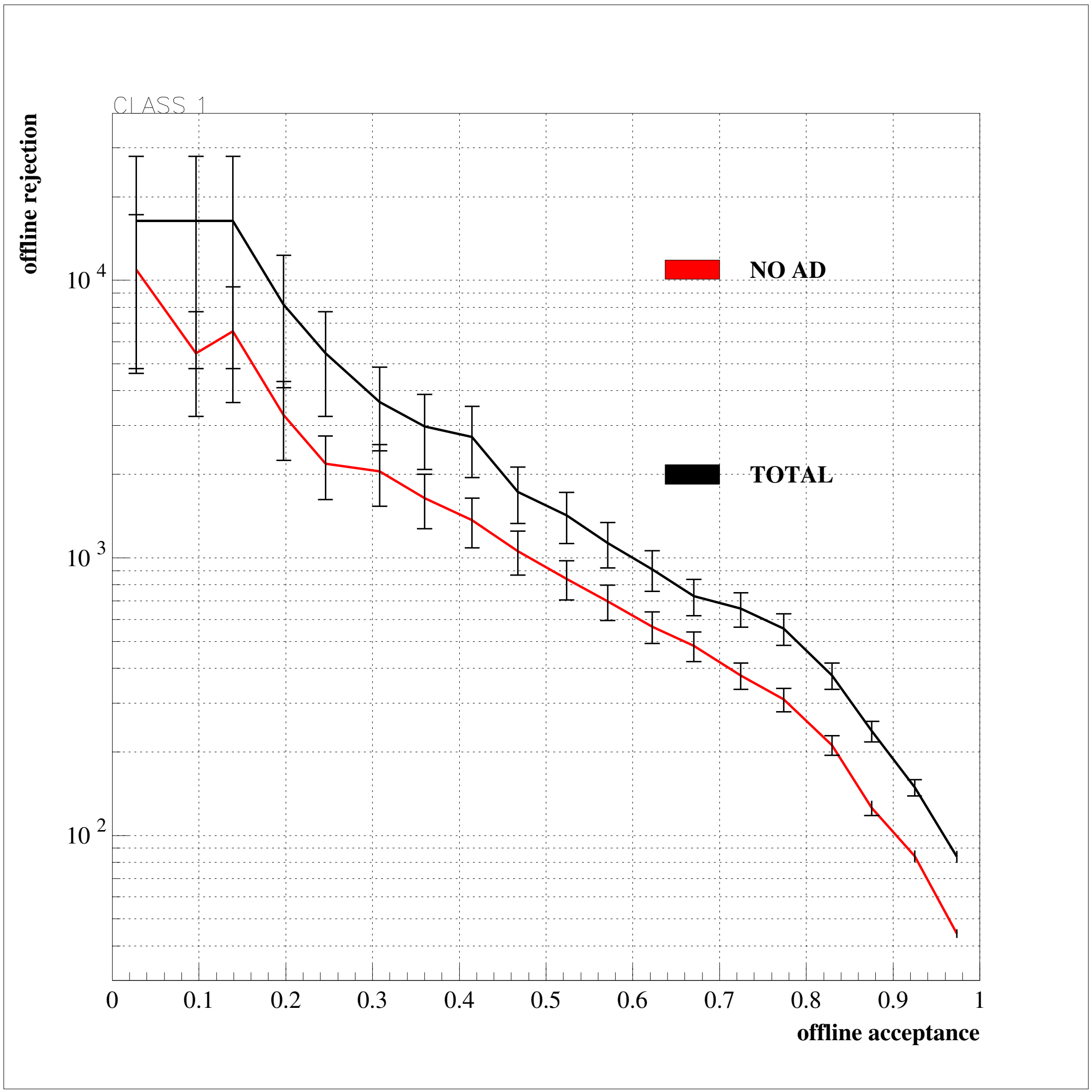

Figure 35: Offline PV rejection vs offline PV acceptance for different tightness for all PV subsystems, with (black) and without (red) the AD, for Kp2 peak events.

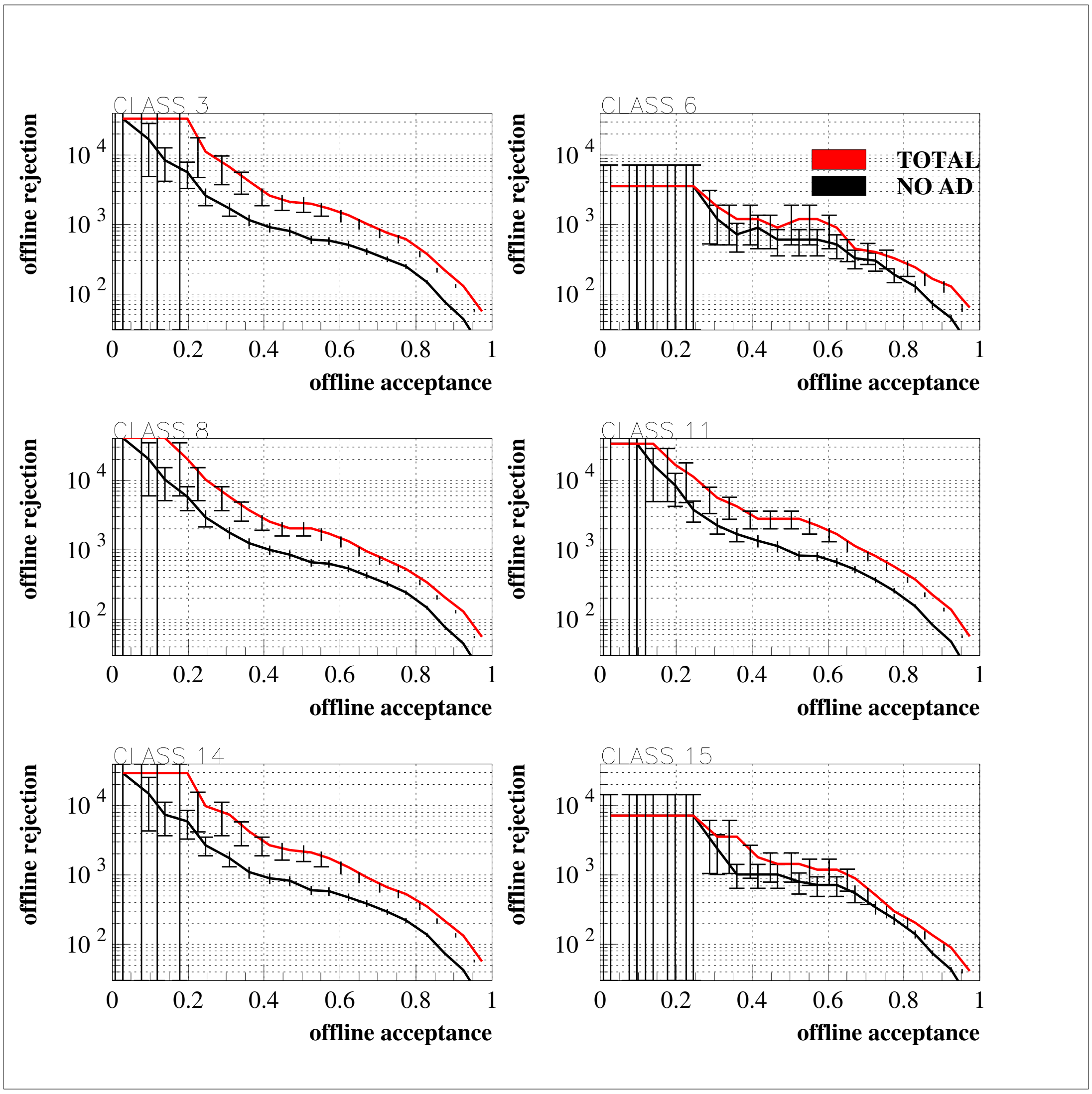

Figure 36: Offline PV rejection vs offline PV acceptance for different tightness for all PV subsystems, with (red) and without (black) the AD, for 6 different classes of PNN2 events. The classes are described in table 10. The upper and/or lower bounds of the error bars that are missing from some points is just a plotting feature.

6 Radial dependence of the energy

The dependence of the energy measured by the AD on the distance of the incoming track from the center of the detector was investigated. This is expected to vary by up to a factor of 2-3, as is shown in fig. 37, where the average (not fitted mean) of the ADC energy distribution of incoming Kaons is ploted vs the distance of the trace of the incoming particle left in the B4 from the center, for Km2 events where the track is confined in one sector. The same trend is present for the CCDs (fig. 38), although the shape variation of the pulse with the distance from the readout may be to blame for the weakest dependence and the saturation for large distances (remember, the CCD "energy" is the pulse height). Unfortunately, any corrections applied to the energy cannot take this radial dependence into account, as there is no track information for particles coming out of the target (unlike beam particles), therefore the radius is unknown. The radial dependence just contributes to the width of any energy peak.

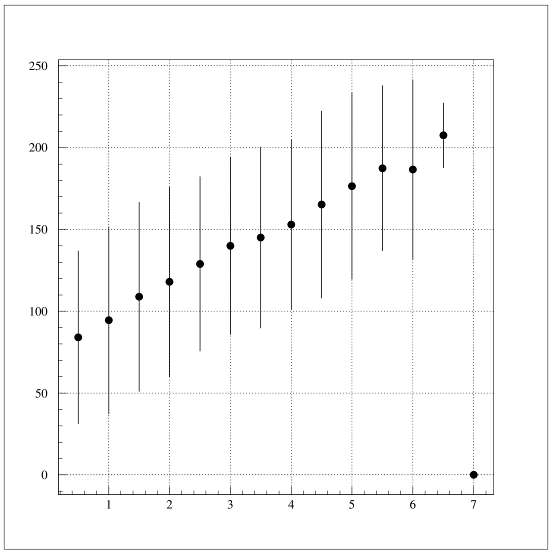

Figure 37: Average of the ADC energy distribution of incoming K's vs the distance of the trace of the incoming particle left in the B4 from the center. The error bars are the sigmas.

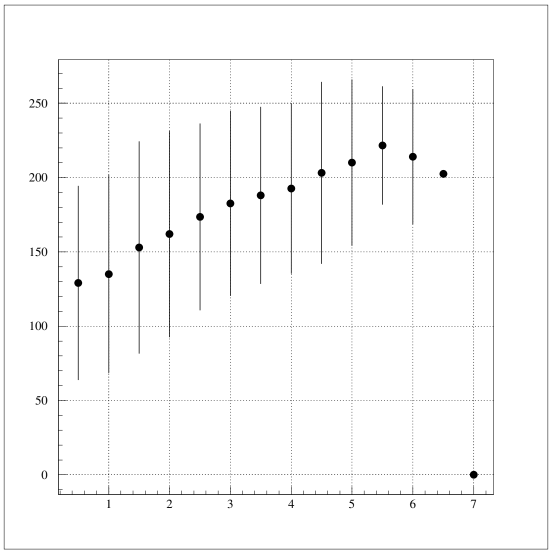

Figure 38: Average of the CCD energy distribution of incoming K's vs the distance of the trace of the incoming particle left in the B4 from the center. The error bars are the sigmas.

References

[1] V.Jain, E787 TN375, "Simulation of elastic scatters of pi+ in the target from Kp2 decays".

[2] D.E. Jaffe, E949 technote K-057, "Estimate of number of photoelectrons in the AD".

[3] Coombes et *al*, E949 technote K-020, "Tests of prototype E949 beam instrumentation".